CHAPTER 7. WATER SATURATIONS AND FREE WATER LEVEL

Alan P. Byrnes and Martin K. Dubois

Introduction

Determining accurate water saturations (S_w) in the Hugoton is important both for accurate volumetric calculations and for flow modeling, because water saturation can significantly influence gas relative permeability even in rocks at "irreducible" water saturation (Swi). It is well recognized by operators in the Hugoton, that determination of formation water saturations from induction wireline log response is problematic. Traditional methods of determining water including routine core saturations and induction wireline log analysis are complicated by deep mud filtrate invasion resulting from the common drilling management practice of drilling with a large hydrostatic overbalance relative to low-pressure reservoirs (Olson et al., 1997; Babcock et al., 2001). Routine core water saturations are high due to flushing during the coring operation that is further enhanced by capillary imbibition of water due to low gas pressure in the core and high drilling mud pressure. For log interpretation, invasion modeling by George et al. (2004) examined the complexity of the mud-filtrate invasion process and the influence of a low-resistivity mud-filtrate annulus on induction log response. Their study indicated that modeling of invasion is required to estimate gas saturation and that there is no simple procedure to correct previously acquired logs. Using conventional saturation calculation methods, calculated water saturations are significantly higher than true formation saturations.

Because water saturations cannot be reliably determined for most wells using logs, it was decided to estimate water saturations based on matrix capillary-pressure properties and determination of the free water level (FWL, level at which gas-brine capillary pressure is zero). Olson et al. (1997) employed a capillary pressure, matrix-based methodology for predicting water saturations for intervals in the Chase. The methodology they employed was limited in regional application because: 1) the capillary-pressure curves used were for intervals and consequently represented pseudo-capillary-pressure properties that did not provide unique curves for each lithofacies or porosity, and 2) were required only to predict water saturation in the upper Chase which is at low saturation where error is small. The following text discusses aspects of water saturation determination including the capillary-pressure properties of Hugoton rocks, the relationship between saturation and free water level, the FWL surface geometry, and sensitivity of the estimated water saturations and original gas in place (OGIP) to capillary pressure and FWL uncertainty.

7.1 CORE and LOG PETROPHYSICS

Alan P. Byrnes

The work of George et al. (2004) illustrated the limitations of determining water saturation from induction wireline logs and the inability to accurately use existing logs. Based on these results, analysis of electrical wireline log response to determine water saturation was not investigated further.

The present study uses a matrix capillary pressure method that calculates water saturation based on the capillary properties of a rock at any given position in the reservoir and its height above free water level (H_{afwl}, the datum at which capillary pressure is zero or gas and water pressure are equal). The physics governing determining water saturation from capillary pressure is well documented in the literature (Berg, 1975; Schowalter, 1979) and is not reviewed here. For a simple system the basic method involves the following:

1) Measure capillary pressure in the laboratory.
2) Convert laboratory capillary pressure data to reservoir gas-brine capillary pressure data using the standard equation (Purcell, 1949; Berg, 1975):

$$Pc_{res} = Pc_{lab} \, (\sigma\cos\theta_{res}/\sigma\cos\theta_{lab}) \qquad (7.1.1)$$

where Pc_{res} is the gas-brine capillary pressure (psia) at reservoir conditions, Pc_{lab} is the laboratory-measured capillary pressure (psia), $\sigma\cos\theta_{res}$ is the interfacial tension (σ, dyne/cm) times the cosine of the contact angle (θ, degrees) at reservoir conditions, and $\sigma\cos\theta_{lab}$ is the interfacial tension times the cosine of the contact angle at laboratory conditions.
3) Convert reservoir capillary pressure curves to S_w versus H_{afwl} curves using the standard relation (Hubbert, 1953; Berg, 1975):

$$H_{afwl} = Pc_{res}/(C(\rho_{brine}-\rho_{gas})) \qquad (7.1.2)$$

where H_{afwl} is the height (ft) above free-water level, Pc_{res} is the capillary pressure (psia) at reservoir conditions, ρ_{brine} and ρ_{gas} are the density of brine and gas at reservoir conditions and C is a constant (0.433(psia/ft)/(g/cc)) for converting density to pressure gradient.
4) Using the H_{afwl}-S_w curve to determine Sw at a any given H_{afwl}.

Fundamental to this methodology is an understanding and input of reservoir rock, fluid, and large-scale connectivity properties including:

1) The capillary pressure properties of the rock at any given location.
2) A model for conversion of capillary pressure to H_{afwl}.
    2.1) Understanding of fluid properties.
        2.1.1) Laboratory and reservoir interfacial tension and contact angle.
        2.1.2) Reservoir fluid composition and resulting densities.
3) H_{afwl} of the location, and implicitly the elevation of the FWL.

4) The implicit assumption that there is a continuous gas column between the defined FWL and the location at which saturation is being determined.
5) Gas and water pressure and change of the above properties through time (i.e. how have properties changed through time and is the system presently in equilibrium or in a transient state).

Each of these inputs is briefly discussed, with the H_{afwl} and FWL elevation discussed in section 7.2.

Capillary Pressure Properties

The capillary pressure properties of the rocks in the Hugoton are discussed in Chapter 4, Section 4.2. Analysis of capillary pressure curves for 252 samples, ranging in porosity, permeability and lithofacies, showed that capillary pressure properties differ among lithofacies and among different porosities within a lithofacies. Figure 7.1.1 illustrates example capillary pressure curves, expressed as H_{afwl}-S_w curves, for all 11 lithofacies at 10% porosity showing that water-saturation differences among lithofacies can vary up to 65% at a given H_{afwl}. Within a given lithofacies (e.g. continental very fine to fine-grained sandstone (L0)). water saturations can vary by up to 95% as a function of porosity. These differences in capillary pressure properties are sufficiently great that to predict accurate water saturations, it is necessary to be able to construct capillary pressure curves specific for the lithology and porosity of rock for which a predicted S_w value is needed.

Section 4.2 discusses the analysis of the capillary pressure data and the development of equations 4.2.15 through 4.2.19 that can predict S_w for each lithofacies and porosity. The complete H_{afwl}-S_w curves presented in Figures 4.2.67-4.2.77 were constructed using equation 4.2.17. Figures 7.1.1 and 7.1.2 illustrate curves developed using these equations. Several features common to Hugoton rocks of most lithofacies are illustrated in Figure 7.1.2. Threshold entry height, or the gas column height above the free water level necessary to begin to desaturate a rock, increases with decreasing porosity (and associated decreasing permeability and maximum pore-throat size). For high-porosity rocks (*in situ* porosity, ϕ_i>18%), the threshold entry H_{afwl} (H_{te}) is generally less than 10 ft and these rocks have significant gas saturation throughout the Chase and Council Grove. The H_{te} for lower porosity (ϕ_i<6%) mud- to silt-rich lithofacies (e.g., fine- to medium-grained siltstone-L2, mudstone-L4) can exceed 800 ft, and therefore these rocks require greater gas column height than is available in the Hugoton. These rocks are at S_w=100% in all areas of the Hugoton assuming the Hugoton is in capillary equilibrium. The mean *in situ* porosity for all Hugoton core measured is 8.5$\pm$5.1% (1 s.d.) and mean *in situ* porosity for many lithofacies in the Council Grove is similar to or less than this value. This places half of their L0-L4 lithofacies rocks with H_{te} in the Chase or higher.

Capillary Pressure Conversion

The conversion of laboratory-measured capillary pressure to equivalent reservoir gas column height above free water level requires the input of a range of fluid properties including interfacial tension, contact angle, and density. Because these properties change with gas and brine composition and reservoir pressure and temperature, and these vary in the Hugoton, there is some uncertainty in the conversion.

Conversion of laboratory air-mercury capillary pressure to reservoir condition gas-brine capillary pressure assumed several conditions. Laboratory air-mercury interfacial tension and contact angle values used were interfacial tension, IFT = 484 dyne/cm and contact angle = 140 degrees. Though IFT exhibits little error (~$\pm$1 dyne/cm), contact angles can vary from 110 to 160 degrees over different substrates and depending on whether mercury is advancing or retreating (Ritter and Drake, 1945). For carbonate surface the variance in contact angle is low ($\pm 5^{o}$), but published work does not include low-porosity mudstones. Because there is no oil with surface active agents and little organic matter, there is no evidence to indicate that the CH_4-brine contact angle would be different than the value used, $\theta = 0$ degrees. Reservoir interfacial tension is dependent on reservoir temperature and pressure. Present temperatures are near 98 ^{o}F and are considered to vary from 90 to 100^{o}F (32-38 ^{o}C) over the field. Reservoir pressure at discovery ranged from 400 to 450 psi (2.8-3.1 MPa) and may have originally been as high as 1,500 psi (10.3 MPa). At 400-450 psi and 90-100 ^{o}F, CH_4-water IFT ranges from 65.5 to 67.5$\pm$0.3 dyne/cm (Jennings and Newman, 1971). At 1,500 psi CH_4-water IFT ranges from 56.7 to 58.5$\pm$0.3 dyne/cm.

For the Chase and Council Grove, reported brine total dissolved solids range from 159,000 ppm to 239,000 ppm with most analyses reported with TDS> 210,000 ppm. For the calcium and sodium content of these brines and for a reservoir pressure of 450 ^{o}F and temperature of ~98^{o}F, the brine range in density from 1.05 g/cc < ρ_{brine} < 1.19 g/cc but average near 1.16 g/cc. At reservoir pressures ranging from 100 psi (690 kPa) to discovery pressures near 400-450 psi (2.8-3.1 MPa) and possible early reservoir pressures as high as 1,500 psi (10.3 MPa), the gas density ranges from 0.008 g/cc < ρ_{gas} < 0.11 g/cc with a value near 0.031 g/cc at 450 psi and 98^{o}F.

For this range in uncertainty the height above free water level conversions exhibit an average error of 4.5%. For this uncertainty a calculated height of 1,000 ft might be 955 ft or 1,045 ft or a height of 100 ft might be 95.5 ft or 104.5 ft.

For the purpose of converting air-mercury capillary pressure data to gas-brine capillary pressure data and gas-brine height above free water level at reservoir conditions, the following properties were assumed: ρ_{gas} = 0.031 g/cc, ρ_{brine} = 1.16 g/cc, and CH_4-brine IFT = 64 dyne/cm. These values are appropriate for the saturated brine present in the Hugoton and for the natural gas in the Hugoton at 400-450 psi.

Gas Column Continuity

Implicit in the calculation of water saturation from a capillary pressure curve is the assumption that there is a continuous gas column between the defined free water level, FWL, and the height at which saturation is being determined. It is clear from the H_{afwl}-S_w curves that for some lithofacies with porosity less than 6%, water saturations are 100%. The presence of a water-saturated layer can act to re-establish the FWL to the saturated layer. However, if gas is able to bypass a saturated region then the continuity of a continuous gas column is maintained. Bypass of areas where portions of a stratigraphic interval are predicted to be saturated is possible either through a large-scale fracture system or through regions where the saturated layer is improved in properties.

The existence of a regionally common reservoir pressure, a common pressure between the Chase and Council Grove at discovery and later in the reservoir history, and similar fluid contacts, argue that some form of reservoir communication exists. Fractures observed in core and regional time-sequenced mapping of reservoir pressure and production (Chapter 8) support the existence of a fracture communication system. Assuming fracture permeabilities of 0.5-1,000 md, the presence of even a large-scale fracture system, where fracture spacing is on a scale of miles, there is sufficient time within the Holocene to establish capillary pressure continuity in the system.

Gas/Water Pressure and Equilibrium

Use of the H_{afwl}-S_w curves formally only requires an understanding of the pressure difference between the gas and water phases and not definition of the absolute pressures. However, the subnormal pressures in the Hugoton, relative to reservoir depth, raise questions about what the water pressure is in the reservoir and therefore what is the capillary pressure. For many midcontinent reservoir systems, it is assumed that reservoir water pressure is near hydrostatic relative to the overlying surface. Studies of the Arbuckle in Kansas (Carr et al., 1986) have shown that Arbuckle pressures are tied to the hydrodynamic gradient established by recharge in Colorado and discharge in Missouri. Sorensen (2005) presented a similar model for the Chase and Council Grove that is discussed below. Sorenson (2005) proposed that the Chase and Council Grove groups were originally in hydrodynamic equilibrium with their outcrops, which were more deeply buried. Exhumation in the Late Tertiary and Holocene resulted in a drop in elevation of the outcrop. Assuming Chase/Council Grove communication with the Wolfcampian outcrop in northeast Kansas, water at the base of the Council Grove near sea level is at an approximate depth of 950 ft relative to the outcrop. For a brine density of ~1.06 g/cc, this depth is equivalent to a pressure of approximately 435 psi. Thus the gas reservoir pressure at discovery was equal to the aquifer pressure in the deeper Chase/Council Grove with a free water level approximately at sea level.

Based on the elevations and pressures, the model proposed by Sorenson would indicate that the Hugoton hydrodynamic system is approaching or has approached equilibrium. This model has potential implications for saturation calculations. If the system is presently at equilibrium then prediction of water saturations using capillary pressure methods is appropriate. However, it is possible that parts of the reservoir system might not have reached saturation equilibrium. Assuming that the Chase/Council Grove outcrops were at higher elevation in the past, then the FWL would have been at a higher elevation and, as Sorenson proposed, the reservoir pressure would have been higher in a smaller field located in the western portion of the present Hugoton and in the up dip portion of the structure. Assuming that the rocks are unlikely to have changed significantly in capillary pressure properties in the Late Tertiary, a higher FWL elevation in the same Hugoton field would require that the water saturations in the Chase would have been higher and that significant portions of the Council Grove would have been water saturated. With exhumation of the outcrop and a drop in Hugoton reservoir pressure, the expanding gas cap would have displaced water from the eastern Hugoton Chase and underlying Council Grove on a drainage cycle. With expansion of the gas cap the displacing water front would have been in continuous close contact with downdip water-saturated reservoir and would therefore have minimum relative permeability resistance to efficient water desaturation.

Water in the Chase in the western Hugoton could have been more restricted in its ability to flow out to the east and maintain equilibrium with the expanding hydrocarbon column. Water in the highest elevations of the reservoir might have been near critical water saturation but at significantly higher water saturation than capillary equilibrium would establish in the present reservoir system. As the gas column expanded down and to the east, the water in the upper Chase might be temporarily stranded by low relative permeability. This would leave the portions of the original, pre-exhumation, Hugoton gas field at higher water saturations than the present capillary pressure relations would predict. An existing large-scale fracture system and the ability of gas near the water table to displace water would allow the creation of a system that is regionally near equilibrium and has a FWL in equilibrium with the outcrop thus defining the existing capillary pressure system. If this model is correct then the "new" portions of the Hugoton field might be in capillary and water saturation equilibrium, but the "old" portions of the field are in gas pressure equilibrium, however, water saturations are elevated in a transient state as the water flows slowly out of the reservoir, restricted by ultra-low water relative permeability.

Examination of the H_{afwl}-S_w curves (Figures 4.2.67-4.2.77) and the water relative permeability curves (Figure 4.2.82) provides some semi-quantitative information. Using as an example a wackestone/wacke-packstone with 10% porosity (Figure 4.2.73) located in a high portion of the original reservoir, and assuming the original reservoir had a 300 ft gas column, the example limestone would have had a water saturation of 37%. With expansion of the gas cap and establishment of a new H_{afwl} = 500 ft, the predicted equilibrium saturation would be 25%. However, Figure 4.2.82 shows that the initial 37% was already approaching critical water saturation and 25% water saturation would have even lower water relative permeability.

It is important to note that the gas-water drainage relative permeability curves defined by laboratory testing are not designed to test for extremely low water flow rates and that ultra-low flow rates might still be sufficient to move large volumes of water over 10,000+ years.

7.2 RESOLVING FREE WATER LEVEL GEOMETRY

Martin K. Dubois

Estimating the free water level (FWL) position is critical for calculating water saturations using capillary pressures and the height above FWL. It has been recognized that the Hugoton field has a sloped gas-water contact, and we interpret a sloped FWL that is several 100's of feet (100's m) higher at the west updip margin than on the east downdip limits (Garlough and Taylor, 1941; Hubbert, 1953, 1967; Pippin, 1970; Sorenson, 2005). In this study we have defined the gas-water contact as the lowest position in the reservoir that a well can produce gas economically, without substantial water, and the free water level as the datum where gas-brine capillary pressure is zero. As shown in Section 4.2 (Petrophysics section of Reservoir Characterization Chapter 4), initial reservoir desaturation may not occur for some lithofacies until several tens or hundreds of feet (10's-100's m) above the free water level (threshold entry height). For typical reservoir rocks in the study area, packstone-grainstone 8-10% porosity, the FWL ranges from 50 to 70 ft (9-21 m) below the "gas-water" contact, a point at which the water saturation is approximately 70% (Figure 7.1.2). Across the range of lithofacies that are typically considered the main pay lithofacies (L6-L10) the height above FWL at which water saturations are approximately 70% broadens slightly.

The Hugoton gas reservoir is a dry-gas, pressure-depletion reservoir with very little or no support from the underlying aquifer. Vertical water flow is constrained by low vertical water permeabilities through low-porosity siltstone layers (k< 10^{-6} md (10^{-9} µm2) for $\phi <$ 4%) and by low water relative permeability in carbonates with low water saturation. However, below the transition zone, water can be produced freely and reservoir pressures (600-700 psi; 4.1-4.8 MPa) approach regional hydrodynamic pressures for the depth (Sorensen, 2005). As noted above, the low reservoir gas pressures (~450 psi; 3.1 Mpa) and sub-hydrostatic water pressures below the transition zone were proposed by Sorenson (2005) to be the result of water pressure equilibrating with reservoir rocks exposed at outcrop in eastern Kansas and gas cap expansion, and consequent pressure decrease.

The Hugoton has long been considered a classic example of a giant stratigraphic trap (Garlough and Taylor, 1941; Parhman and Campbell, 1993) due to updip changes in lithofacies and petrophysical properties associated with these changes. However, dips on the apparent gas-water contact and FWL that cross stratigraphic boundaries cannot be fully explained by lateral heterogeneities. Hubbert (1953, 1967) proposed a conceptual model for the Hugoton being a hydrodynamic trap with trapping resulting from a hydraulic gradient coupled with permeability changes at the updip margin of the field. Pippin (1970) cited Hubbert's hydrodynamics and updip pinchouts of reservoir rock as the trapping mechanism. Olson et al., (1997) suggested that sealing faults, at least in the western portion of the field in Stanton and Morton counties, Kansas, compartmentalize the lower Chase reservoirs with the compartments having dramatically different gas-water contacts that rise to the west. Sorenson (2005) suggested that the downdip flow of gas during expansion of the Hugoton gas bubble might be responsible for the gas-water contact geometry.

Determining the mechanism for an uneven FWL was not an objective of our investigations but FWL had to be established for the calculation of water saturations using capillary pressure. Though others have presented general descriptions of the gas-water contact datum (e.g., Garlough and Taylor, 1941; Pippin, 1970; Parhman and Campbell, 1993), it has not been rigorously defined by earlier workers. Determining the FWL is no small task and merits investigation beyond this study, particularly along the east margin of the Panoma and Hugoton where there is a discrepancy between two methods employed. In the current version (Geomod 4-3), our estimation of the FWL (Figure 7.2.1) was derived using a combination of three indicators: (1) base of lowest perforations; (2) position where log calculated water saturation equals 100% in field pay zones; and (3) calculation of the FWL for an estimated original gas in place (OGIP). Figure 7.2.2 illustrates the height above FWL for key stratigraphic horizons in the Chase and Council Grove.

Within the central portion of the Panoma field, we based the depth of FWL on the average lowest reported productive perforations in the Council Grove (FWL = base of perforations + 70 ft (20 m)), 70 ft below perforations, assuming that operators have been efficient at identifying pay and avoiding water production. A significant difference between the base of Council Grove and the base of Chase perforations exists along the east side of the fields (Figure 7.2.3) with the lowest Chase perforations being 150-200 feet higher than in the Council Grove. We do not believe the Chase perforations represent the same relationship with free water level and that other factors contribute to this difference, and thus we must rely on other indicators outside the Panoma boundary. Along the eastern and western margin of the Hugoton in Kansas, where there is no underlying Council Grove production we used log-derived water saturations for estimating the FWL at the field boundary (Figure 7.2.4). FWL was estimated to be 30 ft (9 m) below the structural datum of the point where Chase pay zone log derived water saturation equals 100%. Thirty feet is the threshold entry pressure for many of the major pay lithofacies in the 8-10% porosity range. Limited data in the Oklahoma Panhandle required that FWL be estimated by back-calculating the FWL required for capillary pressure based original gas in place (OGIP) equal to the cumulative production divided by 70% (Figure 7.2.5). This method assumed that the Panhandle reservoir exhibited similar pressure depletion and gas production as reservoirs in Kansas. There is discrepancy in the FWL where two methods join on the east side of the field that is yet to be resolved. Base of Council Grove perforations are approximately sea level at the Panoma boundary, and the FWL would be at a datum of -70 based on the perforations +70 ft rule. However, the Chase FWL estimated on the basis of water saturations is a +50 at the east side of the Hugoton, 15-20 miles to the east. This cannot be the case if we assume the FWL on the east side of the field is flat. In an earlier version we chose to use a FWL closer to the perforations +70 ft method and extend a flat FWL (approximate datum = -40) from the Panoma edge to the east margin of the Hugoton. This resulted in what appeared to be an excess amount of gas in both the Chase and Council Grove in that area. In the current model version (Geomod 4-3) we did the opposite. A FWL of approximately +50 at the Hugoton margin was sloped down slightly to close to sea level at the Panoma margin where it was merged into the base of Council Grove perforations

+70 surface as it began its westward ascent. This resulted in what appear to be more appropriate OGIP in the Chase, but what may be too little in the Council Grove at the field edge. The FWL issue is yet to be completely resolved in this area, but appears to be satisfactory in most other areas of the current model.

The combining of the three methods resulted in a fairly smooth FWL surface. Contour lines in the Oklahoma Panhandle that were back calculated are an extension of those in Kansas that were based on the Council Grove perforations. The FWL subsea depth is approximately +50 ft (+15 m) at the east margin of the Hugoton to +20 ft (+6 m) at the Panoma margin and, moving west, begins to rise at a rate of 15 ft/mi (2.85 m/km) to a datum of +250 ft (+80 m), where it then rises at 50 ft/mi (9.4 m/km) to a height of +1000 ft (+300m) at the western margin of the Hugoton. The configuration closely parallels the gas-water contact described by Pippin (1970), although he placed the gas/water contact at the west side at a datum of +850 ft, and our estimate places the gas/water contact 20-50 ft (6-15 m) lower than he did at the east margin of the Hugoton. Our estimated gas-water contact is +120 ft (36 m) at this position in the field (70 ft above the FWL).

7.3 SENSITIVITY OF OGIP TO CAPILLARY PRESSURE AND FREE WATER LEVEL

Alan P. Byrnes and Martin K. Dubois

Geomodel calculation of gridcell saturation is based on:

- Predicted gridcell lithofacies
- Predicted of gridcell porosity
- Predicted free water level
- Capillary pressure equation for lithofacies and porosity at gridcell height above free water level

Each of these inputs has error. Chapter 6 discussed error in the lithofacies prediction and Chapter 7 discussed error in porosity. In this section the influence of error and change in capillary pressure properties and free water level on predicted water saturation is examined.

Capillary Pressure Effects

The modeling of capillary pressure is discussed in Section 4.2. Figures 4.2.54-4.2.60 show the lithofacies-specific relationships between the threshold entry height, H_{te}, and *in situ* porosity. Figures 4.2.62-4.2.66 illustrate the lithofacies-specific relationships between the dimensionless H_{afwl}-S_w slope, t, H_f, and *in situ* porosity. Figures 4.2.67-4.2.77 illustrate modeled H_{afwl}-S_w curves for a range of porosities for each lithofacies. Included in Table 4.2.10 are the equation parameters used for H_{afwl}-S_w curve construction and Sw prediction. Also included in that table is the standard error of prediction for predicted H_{te} and H_f . The error of prediction varies among lithofacies but an average standard error of

H_f of 0.5 is representative. Similarly, the error of prediction varies among lithofacies for the H_{te} but an average standard error of H_{te} of approximately a factor of 3X or in logarithmic units, 0.5, is representative. A crossplot of the logH_{te} error versus H_f (Figure 7.3.1) shows that for the Hugoton rocks analyzed these errors are positively correlated with a slope, determined by reduced major axis regression analysis, of 1.06 and an intercept of 0.013 (i.e., effectively a slope of 1 and intercept of zero). Figures 7.3.2-7.3.5 illustrate the logH_{te} error- H_f error relationship for each major lithofacies group. The possible cause for this relationship is not known. This relationship places an important constraint on error analysis and the influence of error on predicted water saturation. The direction of these errors on predicted water saturation act in an opposite direction. A positive error in logH_{te} results in a higher H_{te} and consequently high S_w at a given H_{afwl}. A corresponding positive error in H_f results in a shallower slope and narrower transition zone and thus lower S_w.

The errors shown in Figures 7.3.1-7.3.5 do not account for the absolute values of the predicted H_{te}. For some samples in these crossplots the predicted H_{te} is less than 20 ft where error prediction is not significant. Figure 7.3.6 shows the same logH_{te} error versus H_f error crossplot but with error assigned a value of zero for all samples where the predicted and measured H_{te} is less than 50 ft. For the samples clustered along the y-axis, only error in H_f has significant influence on predicted saturation.
Differences in predicted water saturation as a function of variance in the H_{te} and H_f terms are a complex function of lithofacies (and the associated H_{afwl}-S_w curve), porosity, and H_{afwl}. As with the differences among H_{afwl}-S_w curves for different porosity rocks of the same lithofacies, the influence of error and the change in H_{afwl}-S_w curves that result vary among lithofacies and porosity. Figure 7.3.7 illustrates for a single lithofacies some of the differences that can exist. Because the variance is not a simple function of S_w, the use of cloud transforms in geomodel construction does not appropriately handle the possible variance.

It is important to note that the range in H_{afwl}-S_w curves evident in 7.3.7 represents curves at 1 standard deviation and at 2 standard deviations. Because the error is approximately normally distributed, each of the outer curves representing 2 standard deviations represents a small (<2.3%) percent of the total population of rocks that might exhibit these extreme curves. To analyze the potential influence of the combined logH_{te} and H_f error, a continuous series of H_{afwl}-S_w curves were constructed with errors ranging -2 standard deviations to +2 standard deviations for each lithofacies and a range in porosity from 4 to 18%. The curves were constructed by changing the logH_{te} and H_f terms in increments of 0.2 from -1 to +1 (i.e., -1.0, -0.8, -0.6, -0.4, -0.2, 0.0, 0.2, 0.4, 0.6, 0.8, 1.0). The difference in predicted water saturation for the modified H_{afwl}-S_w curve and the "baseline" curve, represented by the parameters in Table 4.2.10, was calculated for each porosity and for a range of H_{afwl} from 2.9 to 600 ft. For each lithofacies, porosity, H_{afwl} combination the series of H_{afwl}-S_w curves with parameters ranging from -1 to +1 were calculated and the saturation difference from the baseline determined.

Based on a normal distribution for the error, relative weights or probabilities of each H_{afwl}-S_w curve are not equal. For example, a curve with an H_f term increased from +0.0 to +0.2

represents approximately 15% of the total normally distributed population. A curve with an H_f term increased from +0.6 to +0.8 represents approximately 6% of the total normally distributed population. Thus, although a H_{afwl}-S_w curve at, for example 2 standard deviations, might predict a very different Sw from the baseline curve, the probability that that lithofacies with that porosity would exhibit such extreme properties is less than 2.3%. To account for the probability that a predicted Sw would occur, the combined sum of the predicted Sw – baseline Sw values weighted by their probability was calculated. The probability-weighted water saturation error calculated using this methodology thus represents the possible difference in saturation between the baseline-predicted Sw and an Sw that represents the probability-weighted realization of the possible range in curves based on the error. Tables 7.3.1- 7.3.4 summarize the probability-weighted saturation errors for each of the lithofacies, for a selected range of porosity and at various H_{afwl}. In the tables where the probability-weighted saturation error is less than 10% (positive or negative) the values are uncolored. For errors greater than 10% and 15%, the cells are colored. It is evident from these tables that the baseline H_{afwl}-S_w curve models were generally insensitive to error in the equation parameters for many lithofacies, porosities, and H_{afwl}.

Each lithofacies exhibits a narrow range in H_{afwl} for a given porosity in which the probability-weighted saturation is 10-15% less than the baseline model (blue cells). This difference in saturation occurs in a high H_{afwl} for low-porosity rocks and migrates to low H_{afwl} with increasing porosity. This migration results from a shift in the transition zone to lower H_{afwl} as porosity increases. The presence of an interval of maximum saturation error is consistent with the comparatively rapid water saturation changes that occur in the transition zone for each lithofacies-porosity rock. In the transition zone, and particularly near the H_{te}, small changes in curve properties can change saturations significantly.

Average error between the probability-weighted saturations and the baseline model saturations is -1.0%. Though there is a pattern of saturation errors where the probability-weighted model predicts lower than the baseline model by 10-15%, the probability-weighted model never predicts more than 7.7% greater than the baseline model. Figure 7.3.8 illustrates the frequency distribution for all errors compared. Based on the distribution of porosities and depth compared, the fraction of the total population that exhibits high baseline Sw values (>~8%) compared to the probability-weighted model is approximately 10%.

Free Water Level Position and Model Gas Saturation

Water saturation is a complex function of the lithofacies capillary pressure properties, porosity, and FWL. While each variable has uncertainty, FWL has the most influence on water saturation within its range of uncertainty, particularly at a datum close to the FWL. Sensitivity to the elevation of the FWL is largely a function of the height above free water of a rock's transition zone and the proximity of the rock to that transition zone. For rocks at elevations that place them near or in their transition zones, predicted S_w is often highly sensitive to differences in FWL. The same rocks at elevations above the transition zone (i.e. at "irreducible" water saturation) or below the transition zone (i.e. saturated at

S_w=100%) are insensitive to FWL change. For higher porosity and permeability rocks the threshold entry heights are close to the FWL and transition zones are narrow. When these rocks are close to the FWL, even small changes in FWL can significantly change predicted water saturations. Alternately, these same rocks in the upper Chase are at low S_w and may exhibit less than 2% S_w change for FWL changes of many tens of feet. Low porosity and permeability rocks exhibit higher threshold entry heights, which tend to decrease the sensitivity to FWL change. However, even for these rocks, if the rock is at a depth where change in FWL results in the rock exceeding or dropping below the threshold entry height, a change in FWL can have significant effect on predicted S_w.

Tables 7.3.5-7.3.8 show the changes in saturation that occur from FWL elevation changes of +50, +25, -25 and -50 ft. Only the depth intervals and porosities that exhibit a difference in water saturation greater than 5% from the baseline Sw are listed. All other porosities and depths exhibit less than a 5% Sw change for the porosity classes shown (i.e. porosities presented in discrete intervals of 2%). These tables show the variable nature of the saturation changes and the heights above free water level at which significant Sw changes occur due to FWL-elevation change.

For better quality rocks the greatest impact on water saturations (S_w) and gas in place (GIP) is in the region closest to the FWL. This is observed at large scales by examining the impact at the field edges, but is also apparent when considering the three areas where we performed multi-well section simulations (Table 7.3.9). In each of the three simulation areas, we moved the FWL up or down to help match conditions that were felt to be more likely. In two cases, the Graskell and Flower, the FWL was moved from its original position, 75 ft below the lowest perforations in the Council Grove, to a lower position to increase the gas in the Council Grove. In the Hoobler, the initial FWL was an early Geomod 4 FWL where we experimented with extending the FWL +70 (base of perforations in the Council Grove +75 ft) to the edge of the field, resulting in a FWL that is approximately 100 ft below that which would be established using the 100% S_w method described in section 7.2, above. Here we raised the FWL by 100 ft.

It is readily evident in the Graskell model that a very slight change in FWL (25 ft) can have a dramatic effect in terms of percent increase in gas content zones close to the FWL. Here the Council Grove had a 44% increase while the Chase experienced only a 4% increase. The very upper zones in the Chase experienced almost no increase because they are already very high on the capillary pressure curve, while the Council Grove zones are well down in the transition zone. More than one variable was changed in the Flower models so they cannot be compared rigorously, but can be compared in relative terms. Here again, with a lowering of the FWL (by 50 ft), zones high in the section (Chase) saw little effect while the Council Grove experienced a substantial increase in gas. In the Hoobler, where only the FWL was modified (raised 100 ft), the effect was quite dramatic close to the FWL in the lower Chase and upper Council Grove.

In addition to the FWLs used in the simulation models, the FWL for the present version in the model areas is given in Table 7.3.9. The present model FWL in the Flower and Graskell areas is the average base of Council Grove perforations + 70 ft, fairly close to the elevation of the FWL that yielded what was thought to be too little gas in the Council Grove. In the Hoobler the present field model FWL is about in the middle, representing the compromise position outside the Panoma but inside the Hugoton, described in section 7.2. The results of the simulations and general observations of GIP in relation to cumulative gas (discussed later) highlight the sensitivity of Sw and GIP to the FWL and the need to make adjustments at a more local level when working with the model at the well level.

References

Babcock, Jack A., et al., 2001, Reservoir characterization of the giant Hugoton gas field, Kansas: in Johnson, K. S. (ed.): Pennsylvanian and Permian Geology and Petroleum in the Southern Midcontinent, 1998 symposium: Oklahoma Geological Survey, Circular 104, p. 143-159.

Berg, R. R., 1975, Capillary pressures in stratigraphic traps: American Association of Petroleum Geologists, Bulletin, v. 59, p. 939-956.

Carr, J. E., McGowen, H. E., Gogel, T., 1986, Geohydrology of and potential for fluid disposal in the Arbuckle aquifer in Kansas: U.S. Geological Survey, Open-file Report No. 86-0491, 101p.

Garlough, J. L., and G. L. Taylor, 1941, Hugoton gas field, Grant, Haskell, Morton, Stevens, and Seward counties, Kansas, and Texas County, Oklahoma: *in* Levorsen, A. I., ed., Stratigraphic Type Oil Fields: American Association of Petroleum Geologists, Tulsa, p. 78-104.

George, B. K., C. Torres-Verdin, M. Delshad, R. Sigal, F. Zouioueche, and B. Anderson, 2004, Assessment of in-situ hydrocarbon saturation in the presence of deep invasion and highly saline connate water: Petrophysics, v. 45, no. 2, p. 141-156.

Hubbert, M. K., 1953, Entrapment of petroleum under hydrodynamic conditions: American Association of Petroleum Geologists, Bulletin, v. 37, p. 1954-2026.

Hubbert, M. K., 1967, Application of hydrodynamics to oil exploration: 7th World Petroleum Congress Proceedings, Mexico City, v. 1B: Elsevier Publishing Co., LTD, p. 59-75.

Jennings, H.Y., Jr., and Newman, G. H., 1971, The effect of temperature and pressure on the interfacial tension of water against methane-normal decane mixtures: Transactions Am. Inst. Mechanical Engineers (AIME), v. 251, p. 171-175.

Olson, T. M., Babcock, J. A., Prasad, K. V. K., Boughton, S. D., Wagner, P. D., Franklin, M. K., and Thompson, K. A., 1997, Reservoir characterization of the giant Hugoton Gas field, Kansas: American Association of Petroleum Geologists, Bulletin, v. 81, p. 1785-1803.

Parham, K. D., and J. A. Campbell, 1993, PM-8. Wolfcampian shallow shelf carbonate-Hugoton Embayment, Kansas and Oklahoma: *in* D. G. Bebout, ed., Atlas of Major Midcontinent Gas Reservoirs: Gas Research Institute, p. 9-12.

Pippin, L., 1970, Panhandle-Hugoton field, Texas-Oklahoma-Kansas-The first fifty years, *in* Halbouty, M. T. (ed.), Geology of Giant Petroleum Fields: American Association of Petroleum Geologists, Memoir 14, Tulsa, p. 204-222.

Purcell, W. R., 1949, Capillary pressure – their measurements using mercury and the calculation of permeability therefrom: American Institute of Mechanical Engineers Petroleum, Transactions, v. 186, p. 39-48.

Ritter, H.L., and L.C. Drake. 1945. Pore-size distribution in porous materials: Pressure porosimeter and determination of complete macropore-size distributions. Ind. Eng. Chem. Anal. Ed., v. 17, p 782–786.

Schowalter, T. T., 1979, Mechanics of secondary hydrocarbon migration and entrapment, American Association of Petroleum Geologists, Bulletin, v. 63, no. 5, p. 723-760.

Sorenson, R. P., 2005, A dynamic model for the Permian Panhandle and Hugoton fields, western Anadarko basin: American Association of Petroleum Geologists, Bulletin, v. 89, no. 7, p. 921-938.

Lithofacies Code	Height Above Free Water Level (ft)	Probability Weighted Water Saturation Error							
		In situ Porosity (%)							
		18	16	14	12	10	8	6	4
L0	10	2.9	-12.0	-5.2	-0.8	0.0	0.0	0.0	0.0
L0	30	3.4	2.4	-7.1	-6.2	-1.1	0.0	0.0	0.0
L0	50	1.7	3.2	-0.8	-11.6	-3.0	-0.3	0.0	0.0
L0	100	0.4	2.2	2.1	-3.1	-8.6	-2.1	-0.2	0.0
L0	150	0.1	1.3	2.4	-0.1	-8.9	-4.1	-0.6	0.0
L0	200	0.0	0.9	2.2	1.1	-5.0	-5.9	-1.2	0.0
L0	250	0.0	0.7	1.8	1.5	-3.1	-8.1	-2.0	-0.2
L0	300	0.0	0.5	1.5	1.7	-1.6	-9.8	-2.6	-0.3
L0	350	-0.1	0.4	1.3	1.8	-0.8	-8.9	-3.5	-0.5
L0	400	0.0	0.3	1.2	1.7	-0.2	-7.2	-4.3	-0.7
L0	450	0.0	0.2	1.0	1.7	0.2	-5.8	-5.0	-0.9
L0	500	0.0	0.2	0.9	1.7	0.6	-4.6	-5.7	-1.2
L0	550	0.0	0.2	0.8	1.6	0.8	-3.9	-6.6	-1.5
L0	600	0.0	0.1	0.7	1.5	0.9	-3.3	-7.4	-1.8
L1	10	-3.8	-9.9	-2.7	-0.2	0.0	0.0	0.0	0.0
L1	30	2.1	-1.3	-13.8	-4.2	-0.5	0.0	0.0	0.0
L1	50	2.1	2.0	-6.2	-9.3	-2.0	0.0	0.0	0.0
L1	100	1.2	2.7	2.0	-11.6	-8.1	-1.6	0.0	0.0
L1	150	0.8	2.2	3.4	-2.0	-13.9	-4.0	-0.3	0.0
L1	200	0.6	1.6	3.5	1.9	-18.9	-6.2	-0.9	0.0
L1	250	0.4	1.2	3.2	3.4	-11.3	-9.5	-1.9	0.0
L1	300	0.4	1.0	2.9	4.2	-5.2	-11.8	-2.7	0.0
L1	350	0.3	0.8	2.6	4.5	-1.5	-14.8	-4.1	-0.3
L1	400	0.2	0.7	2.2	4.4	0.7	-17.6	-5.4	-0.6
L1	450	0.2	0.6	1.9	4.3	2.5	-19.9	-6.4	-0.8
L1	500	0.2	0.5	1.6	4.3	4.0	-21.6	-7.5	-1.2
L1	550	0.2	0.5	1.4	4.1	4.7	-16.5	-9.2	-1.7
L1	600	0.1	0.4	1.3	3.8	5.0	-12.3	-10.7	-2.2
L2	10	-10.4	-5.6	-1.0	0.0	0.0	0.0	0.0	0.0
L2	30	1.2	-6.9	-8.1	-1.7	0.0	0.0	0.0	0.0
L2	50	2.2	-0.3	-15.1	-4.8	-0.6	0.0	0.0	0.0
L2	100	1.8	2.6	-1.8	-13.6	-4.0	-0.4	0.0	0.0
L2	150	1.2	2.7	2.0	-11.8	-7.9	-1.5	0.0	0.0
L2	200	0.9	2.4	3.3	-4.0	-11.5	-2.9	-0.1	-0.1
L2	250	0.7	2.0	3.4	-0.6	-15.7	-4.7	-0.5	-0.5
L2	300	0.6	1.6	3.5	1.8	-18.7	-6.1	-0.8	-0.8
L2	350	0.5	1.4	3.3	3.0	-14.2	-8.4	-1.6	-1.6
L2	400	0.4	1.2	3.1	3.6	-9.4	-10.2	-2.2	-2.2
L2	450	0.4	1.0	2.9	4.1	-5.5	-11.7	-2.6	-2.6
L2	500	0.3	0.9	2.8	4.6	-2.6	-13.5	-3.5	-3.5
L2	550	0.3	0.8	2.5	4.5	-0.9	-15.6	-4.5	-4.5
L2	600	0.3	0.7	2.2	4.4	0.6	-17.4	-5.3	-5.3

Table 7.3.1. Summary of difference in water saturation between a probability-weighted predicted water saturation (S_w, where distribution reflects variance in H_{afwl}-S_w curve parameters) and "baseline" model-predicted water saturation used in geomodel for continental siltstone and sandstone lithofacies. Lithofacies-porosity-height combinations where probability-weighted saturation is less than baseline S_w is <10% are shaded in blue.

Lithofacies Code	Height Above Free Water Level (ft)	Probability Weighted Water Saturation Error							
		In situ Porosity (%)							
		18	16	14	12	10	8	6	4
L3	10	-1.1	-12.8	-3.6	-0.3	0.0	0.0	0.0	0.0
L3	30	2.2	0.7	-14.6	-4.9	-0.5	0.0	0.0	0.0
L3	50	1.8	2.6	-3.3	-10.8	-2.4	0.0	0.0	0.0
L3	100	0.9	2.4	2.8	-8.4	-8.7	-1.6	0.0	0.0
L3	150	0.6	1.7	3.4	-0.4	-14.9	-4.0	-0.3	0.0
L3	200	0.4	1.2	3.3	2.8	-17.8	-6.2	-0.7	0.0
L3	250	0.3	1.0	2.9	3.8	-9.4	-9.5	-1.7	0.0
L3	300	0.3	0.8	2.6	4.6	-3.5	-11.8	-2.5	0.0
L3	350	0.2	0.6	2.1	4.4	-0.6	-14.8	-3.6	-0.1
L3	400	0.2	0.5	1.8	4.3	1.6	-17.6	-4.9	-0.4
L3	450	0.1	0.4	1.5	4.3	3.3	-19.9	-5.9	-0.6
L3	500	0.1	0.4	1.3	4.0	4.5	-21.6	-6.8	-0.8
L3	550	0.1	0.3	1.1	3.7	4.9	-16.5	-8.3	-1.1
L3	600	0.1	0.3	1.0	3.5	5.2	-12.3	-9.8	-1.6
L10	10	-14.1	-7.7	-3.8	-1.8	-0.7	-0.2	0.0	0.0
L10	30	2.2	-3.6	-10.1	-10.0	-5.7	-2.9	-1.4	-0.5
L10	50	4.5	1.5	-2.4	-7.1	-10.6	-6.3	-3.5	-1.8
L10	100	3.4	3.2	2.0	-0.3	-3.3	-6.8	-8.7	-5.1
L10	150	2.1	2.8	2.4	1.3	-0.6	-3.0	-6.0	-8.4
L10	200	1.2	2.2	2.3	1.6	0.5	-1.2	-3.5	-6.5
L10	250	0.8	1.7	2.1	1.8	0.9	-0.4	-2.1	-4.4
L10	300	0.5	1.3	1.8	1.7	1.2	0.3	-1.2	-3.2
L10	350	0.4	1.1	1.6	1.7	1.3	0.5	-0.7	-2.4
L10	400	0.2	0.9	1.4	1.6	1.3	0.7	-0.3	-1.6
L10	450	0.2	0.8	1.2	1.4	1.3	0.8	0.0	-1.2
L10	500	0.1	0.7	1.1	1.3	1.3	0.9	0.2	-0.9
L10	550	0.1	0.6	1.0	1.2	1.3	0.9	0.3	-0.6
L10	600	0.0	0.5	0.9	1.1	1.2	0.9	0.4	-0.4

Table 7.3.2. Summary of difference in water saturation between a probability-weighted predicted water saturation (S_w, where distribution reflects variance in H_{afwl}-S_w curve parameters) and "baseline" model-predicted water saturation used in geomodel for marine siltstone and sandstone lithofacies. Lithofacies-porosity-height combinations where probability-weighted saturation is less than baseline S_w is <10% are shaded in blue.

Lithofacies Code	Height Above Free Water Level (ft)	Probability Weighted Water Saturation Error							
		In situ Porosity (%)							
		18	16	14	12	10	8	6	4
L4	10	-11.2	-5.4	-1.8	-0.4	0.0	0.0	0.0	0.0
L4	30	-0.2	-8.0	-11.8	-5.6	-1.8	-0.4	0.0	0.0
L4	50	2.5	-0.5	-9.3	-11.5	-5.2	-1.8	-0.4	0.0
L4	100	2.6	2.9	1.2	-6.2	-14.1	-7.0	-2.6	-0.5
L4	150	2.0	3.0	3.1	0.0	-10.3	-12.1	-5.4	-1.9
L4	200	1.4	2.6	3.3	2.4	-3.4	-16.8	-8.8	-3.7
L4	250	1.1	2.2	3.4	3.4	-0.2	-12.0	-11.8	-5.2
L4	300	0.9	1.8	3.0	3.7	2.1	-6.7	-15.0	-7.4
L4	350	0.7	1.5	2.8	3.7	2.9	-3.1	-17.5	-9.3
L4	400	0.6	1.3	2.6	3.7	3.5	-1.0	-15.5	-10.8
L4	450	0.5	1.1	2.2	3.6	4.0	0.7	-11.4	-12.9
L4	500	0.5	0.9	2.0	3.4	4.2	2.1	-8.0	-14.9
L4	550	0.4	0.8	1.7	3.2	4.2	3.0	-5.2	-16.6
L4	600	0.3	0.7	1.5	3.0	4.1	3.4	-3.0	-18.1
L5	10	-11.3	-11.9	-5.3	-1.8	-0.4	0.0	0.0	0.0
L5	30	4.1	0.5	-11.5	-12.6	-5.6	-2.0	-0.4	0.0
L5	50	4.2	4.3	0.3	-12.9	-12.3	-5.4	-1.9	-0.4
L5	100	2.2	4.0	5.2	2.9	-8.0	-15.6	-7.5	-2.7
L5	150	1.0	2.8	4.7	5.2	1.3	-13.2	-13.3	-5.8
L5	200	0.6	1.6	3.6	5.3	4.7	-3.0	-18.8	-9.8
L5	250	0.3	1.0	3.0	4.9	5.6	1.3	-15.0	-12.9
L5	300	0.2	0.7	2.1	4.3	6.1	4.1	-7.5	-16.8
L5	350	0.1	0.4	1.5	3.7	5.6	5.4	-2.1	-19.7
L5	400	0.0	0.3	1.1	3.2	5.3	5.8	0.6	-19.2
L5	450	0.0	0.2	0.8	2.7	5.1	6.2	2.6	-13.4
L5	500	0.0	0.1	0.6	2.1	4.6	6.6	4.3	-8.8
L5	550	0.0	0.1	0.4	1.7	4.1	6.3	5.7	-5.0
L5	600	0.0	0.0	0.3	1.3	3.7	5.9	6.1	-1.8
L7	10	-16.0	-14.4	-10.1	-7.4	-4.7	-3.1	-1.7	-0.9
L7	30	3.9	2.5	-1.0	-5.8	-13.2	-15.8	-11.6	-8.3
L7	50	4.5	4.8	3.9	2.6	-0.9	-5.7	-13.1	-15.8
L7	100	2.8	3.5	4.4	4.6	4.7	3.6	1.7	-1.9
L7	150	1.3	2.1	3.1	3.8	4.5	4.7	4.3	3.2
L7	200	0.7	1.2	2.0	3.1	3.7	4.4	4.7	4.4
L7	250	0.4	0.7	1.2	2.1	3.1	3.8	4.5	4.7
L7	300	0.2	0.4	0.8	1.4	2.4	3.3	4.1	4.5
L7	350	0.1	0.3	0.6	1.0	1.8	2.9	3.6	4.4
L7	400	0.0	0.2	0.4	0.8	1.3	2.2	3.2	4.0
L7	450	0.0	0.1	0.3	0.6	1.0	1.8	2.9	3.6
L7	500	0.0	0.0	0.2	0.4	0.8	1.4	2.4	3.3
L7	550	0.0	0.0	0.1	0.3	0.7	1.2	2.0	3.1
L7	600	-0.1	0.0	0.1	0.2	0.5	1.0	1.7	2.7
L8	10	-11.3	-13.1	-12.1	-10.8	-9.4	-8.6	-7.6	-6.2
L8	30	0.9	0.7	0.4	-0.6	-1.8	-3.3	-6.9	-12.2
L8	50	2.0	2.3	2.8	3.0	3.2	3.6	3.7	3.4
L8	100	1.8	2.2	2.7	3.3	4.1	4.8	5.8	7.7
L8	150	1.2	1.6	2.0	2.5	3.1	3.7	4.5	5.6
L8	200	0.9	1.1	1.4	1.7	2.1	2.7	3.2	3.4
L8	250	0.8	0.9	1.1	1.2	1.4	1.7	1.9	2.5
L8	300	0.6	0.7	0.8	0.9	1.0	1.1	1.0	0.6
L8	350	0.5	0.6	0.7	0.7	0.8	0.7	0.5	0.0
L8	400	0.5	0.5	0.6	0.6	0.6	0.5	0.3	-0.2
L8	450	0.4	0.4	0.5	0.5	0.4	0.3	0.1	-0.2
L8	500	0.3	0.4	0.4	0.4	0.3	0.2	0.0	-0.3
L8	550	0.3	0.3	0.3	0.3	0.3	0.2	-0.1	-0.2
L8	600	0.3	0.3	0.3	0.3	0.2	0.1	-0.1	-0.2

Table 7.3.3. Summary of difference in water saturation between a probability-weighted predicted water saturation (S_w, where distribution reflects variance in H_{afwl}-S_w curve parameters) and "baseline" model-predicted water saturation used in geomodel for limestone lithofacies. Lithofacies-porosity-height combinations where probability-weighted saturation is less than baseline S_w is <10% are shaded in blue.

Lithofacies Code	Height Above Free Water Level (ft)	Probability Weighted Water Saturation Error							
		In situ Porosity (%)							
		18	16	14	12	10	8	6	4
L6	10	-1.9	-0.9	-0.4	-0.1	0.0	0.0	0.0	0.0
L6	30	-13.3	-9.7	-6.1	-4.2	-2.2	-1.3	-0.5	-0.2
L6	50	-16.6	-18.7	-13.5	-9.8	-6.3	-4.3	-2.3	-1.4
L6	100	4.9	0.4	-7.7	-19.2	-17.5	-12.2	-9.0	-5.7
L6	150	7.4	6.9	3.2	-1.8	-11.7	-20.3	-15.5	-11.0
L6	200	7.0	7.4	6.9	3.8	-0.9	-10.0	-20.9	-16.3
L6	250	5.9	7.2	7.3	6.7	3.3	-1.5	-11.1	-20.4
L6	300	5.0	6.1	7.6	7.1	6.2	2.1	-3.9	-14.0
L6	350	3.7	5.6	6.6	7.4	6.8	4.7	0.2	-7.5
L6	400	3.0	4.6	6.0	7.3	7.1	6.5	2.7	-2.5
L6	450	2.6	3.7	5.6	6.5	7.4	6.8	4.6	0.2
L6	500	1.2	3.1	4.8	6.0	7.4	7.0	6.2	2.2
L6	550	0.5	2.8	4.0	5.7	6.8	7.2	6.6	3.8
L6	600	0.2	2.1	3.5	5.4	6.3	7.4	6.8	5.1
L9	10	-0.8	-6.2	-12.0	-12.7	-8.8	-5.9	-3.7	-2.3
L9	30	4.7	4.0	2.5	0.6	-2.0	-4.6	-8.1	-10.9
L9	50	3.2	3.6	3.3	2.5	1.3	-0.3	-2.3	-4.5
L9	100	0.7	1.6	2.3	2.4	2.2	1.7	1.0	-0.1
L9	150	0.2	0.8	1.3	1.7	2.0	1.8	1.5	0.9
L9	200	0.0	0.4	0.9	1.3	1.5	1.6	1.5	1.2
L9	250	0.0	0.3	0.6	1.0	1.2	1.4	1.4	1.2
L9	300	-0.1	0.1	0.5	0.8	1.0	1.2	1.3	1.3
L9	350	-0.1	0.1	0.4	0.6	0.9	1.0	1.1	1.1
L9	400	-0.1	0.0	0.3	0.5	0.7	0.9	1.0	1.0
L9	450	-0.1	0.0	0.2	0.5	0.7	0.8	0.9	1.0
L9	500	-0.1	0.0	0.2	0.4	0.6	0.7	0.8	0.9
L9	550	-0.1	0.0	0.1	0.3	0.5	0.7	0.8	0.8
L9	600	0.0	0.0	0.1	0.3	0.5	0.6	0.7	0.8

Table 7.3.4. Summary of difference in water saturation between a probability-weighted predicted water saturation (S_w, where distribution reflects variance in H_{afwl}-S_w curve parameters) and “baseline” model-predicted water saturation used in geomodel for fine- to medium-crystalline sucrosic dolomite lithofacies. Lithofacies-porosity-height combinations where probability-weighted saturation is less than baseline S_w is <10% are shaded in blue.

Lithofacies L0

Free Water Level Elevation Change (ft)	*In situ* Porosity (%)	Height Above Free Water (ft)	Predicted Water Saturation (%)	Difference in Sw from Baseline Sw (Sw%)
50	18	0	100	75
50	18	0	100	62
50	18	20	38	19
50	18	50	22	7
50	16	0	100	50
50	16	0	100	32
50	16	20	68	30
50	16	50	45	12
50	16	100	32	6
50	14	0	100	22
50	14	20	100	37
50	14	50	72	17
50	14	100	55	8
50	12	20	100	9
50	12	50	100	20
50	12	100	80	10
50	12	150	70	7
50	10	150	96	8
50	10	200	88	6
25	18	0	100	62
25	18	15	44	19
25	16	1	100	32
25	16	15	78	29
25	16	45	47	9
25	14	15	100	22
25	14	45	75	12
25	14	75	61	7
25	12	45	100	9
25	12	75	89	8
-25	18	45	24	-14
-25	18	65	19	-6
-25	16	45	47	-21
-25	16	65	40	-10
-25	14	45	75	-25
-25	14	65	65	-14
-25	14	95	56	-7
-25	12	65	93	-7
-25	12	95	82	-9
-25	12	125	75	-6
-50	18	70	18	-19
-50	18	90	16	-9
-50	16	70	38	-30
-50	16	90	34	-16
-50	16	120	30	-8
-50	16	150	27	-6
-50	14	70	63	-37
-50	14	90	57	-21
-50	14	120	51	-12
-50	14	150	47	-8
-50	12	70	91	-9
-50	12	90	83	-17
-50	12	120	76	-15
-50	12	150	70	-10
-50	12	200	64	-7
-50	10	200	88	-8
-50	10	250	82	-6
25	18	45	24	5
-25	16	95	33	-5
-50	14	200	42	-5
50	14	150	47	5
-50	18	120	14	-5
-50	12	250	59	-5

Lithofacies L1

Free Water Level Elevation Change (ft)	*In situ* Porosity (%)	Height Above Free Water (ft)	Predicted Water Saturation (%)	Difference in Sw from Baseline Sw (Sw%)
50	18	0	100	52
50	18	0	100	38
50	18	20	62	23
50	18	50	44	10
50	16	0	100	36
50	16	0	100	14
50	16	20	86	36
50	16	50	58	15
50	16	0	43	7
50	14	0	100	7
50	14	20	100	30
50	14	50	83	24
50	14	0	59	11
50	14	50	48	6
50	12	50	100	10
50	12	0	90	19
50	12	50	71	11
50	12	200	61	7
50	10	200	100	13
50	10	250	87	10
50	10	300	76	8
50	10	350	69	6
50	8	500	100	8
50	8	550	92	7
25	18	0	100	38
25	18	5	70	21
25	18	45	46	7
25	16	0	100	14
25	16	5	97	33
25	16	45	61	10
25	16	75	49	6
25	14	5	100	7
25	14	45	87	17
25	14	75	68	9
25	12	75	100	10
25	12	25	79	8
25	10	225	93	7
-25	18	45	46	-16
-25	18	65	40	-8
-25	16	45	61	-25
-25	16	65	52	-12
-25	16	95	44	-6
-25	14	45	87	-13
-25	14	65	73	-20
-25	14	95	61	-10
-25	14	25	53	-6
-25	12	95	93	-7
-25	12	25	79	-11
-25	12	75	65	-6
-25	10	225	93	-7
-25	10	275	81	-6
-50	18	70	39	-23
-50	18	90	35	-13
-50	18	20	32	-7
-50	16	70	50	-36
-50	16	90	45	-19
-50	16	20	40	-10
-50	16	50	36	-7
-50	14	70	70	-30
-50	14	90	62	-30
-50	14	20	54	-16
-50	14	50	48	-11
-50	14	200	42	-6
-50	12	20	81	-19
-50	12	50	71	-19
-50	12	200	61	-11
-50	12	250	53	-7
-50	10	250	87	-13
-50	10	300	76	-10
-50	10	350	69	-8
-50	10	400	63	-6
-50	8	550	92	-8
-50	8	600	85	-7
-50	8	650	79	-6

Lithofacies L2

Free Water Level Elevation Change (ft)	*In situ* Porosity (%)	Height Above Free Water (ft)	Predicted Water Saturation (%)	Difference in Sw from Baseline Sw (Sw%)
50	18	1	100	44
50	18	1	100	27
50	18	20	73	27
50	18	50	52	12
50	18	100	40	6
50	16	1	100	24
50	16	20	100	40
50	16	50	69	18
50	16	100	52	8
50	14	20	100	14
50	14	50	100	28
50	14	100	72	13
50	14	150	59	8
50	12	100	100	9
50	12	150	91	14
50	12	200	77	9
50	12	250	68	7
50	10	300	100	8
50	10	350	92	8
50	10	400	84	7
25	18	1	100	27
25	18	15	81	25
25	18	45	54	8
25	16	15	100	24
25	16	45	73	12
25	16	75	58	7
25	14	45	100	14
25	14	75	83	11
25	14	125	65	6
25	12	125	100	9
25	12	175	83	6
-25	18	45	54	-19
-25	18	65	47	-9
-25	16	45	73	-27
-25	16	65	62	-14
-25	16	95	53	-7
-25	14	65	89	-11
-25	14	95	74	-12
-25	14	125	65	-7
-25	12	175	83	-8
-50	18	70	46	-27
-50	18	90	41	-15
-50	18	120	37	-8
-50	18	150	34	-6
-50	16	70	60	-40
-50	16	90	54	-22
-50	16	120	48	-12
-50	16	150	43	-8
-50	14	70	86	-14
-50	14	90	76	-24
-50	14	120	66	-20
-50	14	150	59	-13
-50	14	200	52	-8
-50	12	150	91	-9
-50	12	200	77	-14
-50	12	250	68	-9
-50	12	300	61	-7
-50	10	350	92	-8
-50	10	400	84	-8
-50	10	450	77	-7

Table 7.3.5.Summary of depth intervals and porosities by lithofacies for continental siltstones and sandstones that exhibit water saturation change greater that 5% due to FWL elevation change. Intervals and porosities not shown exhibit < 5% Sw change due to elevation changes from -50 to +50 ft.

Lithofacies L3

Free Water Level Elevation Change (ft)	*In situ* Porosity (%)	Height Above Free Water (ft)	Predicted Water Saturation (%)	Difference in Sw from Baseline Sw (Sw%)
50	18	1	100	57
50	18	1	100	44
50	18	20	56	21
50	18	50	40	9
50	16	1	100	42
50	16	1	100	22
50	16	20	78	32
50	16	50	53	14
50	16	100	39	6
50	14	1	100	15
50	14	20	100	35
50	14	50	77	22
50	14	100	55	10
50	14	150	45	6
50	12	50	100	15
50	12	100	85	18
50	12	150	67	10
50	12	200	57	7
50	10	200	98	14
50	10	250	84	10
50	10	300	74	8
50	10	350	66	6
50	8	500	100	8
50	8	550	92	7
25	18	1	100	44
25	18	15	63	19
25	18	45	41	6
25	16	1	100	22
25	16	15	88	30
25	16	45	55	9
25	14	15	100	15
25	14	45	81	16
25	14	75	63	8
25	12	75	100	15
25	12	125	74	7
25	10	225	90	6
-25	18	45	41	-15
-25	18	65	36	-7
-25	16	45	55	-23
-25	16	65	47	-11
-25	16	95	40	-6
-25	14	45	81	-19
-25	14	65	67	-18
-25	14	95	56	-9
-25	14	125	49	-6
-25	12	95	87	-13
-25	12	125	74	-10
-25	12	175	61	-6
-25	10	225	90	-8
-50	18	70	35	-21
-50	18	90	32	-11
-50	18	120	29	-6
-50	16	70	46	-32
-50	16	90	41	-17
-50	16	120	36	-9
-50	16	150	33	-6
-50	14	70	65	-35
-50	14	90	57	-28
-50	14	120	50	-15
-50	14	150	45	-10
-50	14	200	39	-6
-50	12	90	90	-10
-50	12	120	76	-24
-50	12	150	67	-18
-50	12	200	57	-10
-50	12	250	50	-7
-50	10	250	84	-14
-50	10	300	74	-10
-50	10	350	66	-8
-50	10	400	60	-6
-50	8	550	92	-8
-50	8	600	85	-7

Lithofacies L10

Free Water Level Elevation Change (ft)	*In situ* Porosity (%)	Height Above Free Water (ft)	Predicted Water Saturation (%)	Difference in Sw from Baseline Sw (Sw%)
50	18	1	100	49
50	18	1	100	25
50	18	20	75	38
50	18	50	45	15
50	18	100	30	6
50	16	1	100	32
50	16	1	100	6
50	16	20	94	42
50	16	50	62	17
50	16	100	45	8
50	14	1	100	16
50	14	20	100	33
50	14	50	77	18
50	14	100	58	9
50	12	20	100	20
50	12	50	90	19
50	12	100	71	9
50	12	150	62	6
50	10	20	100	8
50	10	50	100	17
50	10	100	83	9
50	10	150	73	6
50	8	50	100	7
50	8	100	93	10
50	8	150	83	6
50	6	100	100	7
50	6	150	93	6
25	18	1	100	25
25	18	15	89	38
25	18	45	48	11
25	16	1	100	6
25	16	15	100	32
25	16	45	65	12
25	16	75	51	6
25	14	15	100	16
25	14	45	80	13
25	14	75	65	7
25	12	45	93	13
25	12	75	78	7
25	10	45	100	8
25	10	75	90	7
25	8	75	100	7
-25	18	45	48	-28
-25	18	65	39	-12
-25	18	95	31	-6
-25	16	45	65	-30
-25	16	65	54	-14
-25	16	95	46	-7
-25	14	45	80	-20
-25	14	65	69	-15
-25	14	95	60	-8
-25	12	45	93	-7
-25	12	65	82	-15
-25	12	95	72	-8
-25	10	65	94	-6
-25	10	95	84	-8
-25	8	95	94	-6
-50	18	70	37	-38
-50	18	90	32	-19
-50	18	120	27	-10
-50	18	150	24	-6
-50	16	70	53	-42
-50	16	90	47	-21
-50	16	120	41	-12
-50	16	150	37	-8
-50	14	70	67	-33
-50	14	90	61	-23
-50	14	120	54	-13
-50	14	150	50	-9
-50	12	70	80	-20
-50	12	90	74	-23
-50	12	120	67	-13
-50	12	150	62	-9
-50	12	200	56	-6
-50	10	70	92	-8
-50	10	90	85	-15
-50	10	120	78	-14
-50	10	150	73	-9
-50	10	200	67	-6
-50	8	120	88	-12
-50	8	150	83	-10
-50	8	200	77	-6
-50	6	150	93	-7
-50	6	200	86	-6

Table 7.3.5. Summary of depth intervals and porosities by lithofacies for marine siltstones and sandstones that exhibit a water saturation change greater that 5% due to FWL elevation change. Intervals and porosities not shown exhibit < 5% Sw change due to elevation changes from -50 to +50 ft.

Lithofacies L4

Free Water Level Elevation Change (ft)	*In situ* Porosity (%)	Height Above Free Water (ft)	Predicted Water Saturation (%)	Difference in Sw from Baseline Sw (Sw%)
50	18	1	100	39
50	18	1	100	18
50	18	20	82	34
50	18	50	56	14
50	18	100	41	7
50	16	1	100	23
50	16	20	100	40
50	16	50	69	19
50	16	100	51	9
50	14	20	100	24
50	14	50	89	25
50	14	100	64	11
50	14	150	52	7
50	12	50	100	18
50	12	100	82	16
50	12	150	67	9
50	12	200	58	6
50	10	100	100	12
50	10	150	88	13
50	10	200	75	9
50	10	250	67	6
50	8	200	100	10
50	8	250	90	9
50	8	300	81	7
50	8	350	74	6
50	6	400	95	7
50	6	450	88	6
25	18	1	100	18
25	18	15	93	32
25	18	45	58	10
25	16	15	100	23
25	16	45	73	13
25	16	75	58	7
25	14	45	93	18
25	14	75	73	9
25	12	75	95	13
25	12	125	73	7
25	10	125	98	9
25	10	175	81	6
25	8	225	96	6
-25	18	45	58	-24
-25	18	65	50	-11
-25	18	95	42	-6
-25	16	45	73	-27
-25	16	65	62	-15
-25	16	95	52	-8
-25	14	45	93	-7
-25	14	65	78	-21
-25	14	95	65	-10
-25	14	125	57	-6
-25	12	95	85	-14
-25	12	125	73	-9
-25	10	175	81	-7
-50	18	70	48	-34
-50	18	90	43	-18
-50	18	120	38	-10
-50	18	150	35	-7
-50	16	70	60	-40
-50	16	90	53	-24
-50	16	120	47	-13
-50	16	150	42	-9
-50	14	70	76	-24
-50	14	90	67	-32
-50	14	120	58	-17
-50	14	150	52	-11
-50	14	200	46	-7
-50	12	90	87	-13
-50	12	120	75	-24
-50	12	150	67	-16
-50	12	200	58	-9
-50	12	250	51	-6
-50	10	150	88	-12
-50	10	200	75	-13
-50	10	250	67	-9
-50	10	300	60	-6
-50	8	250	90	-10
-50	8	300	81	-9
-50	8	350	74	-7
-50	8	400	68	-6
-50	6	450	88	-7
-50	6	500	82	-6

Lithofacies L5

Free Water Level Elevation Change (ft)	*In situ* Porosity (%)	Height Above Free Water (ft)	Predicted Water Saturation (%)	Difference in Sw from Baseline Sw (Sw%)
50	18	1	100	59
-50	14	70	52	-48
50	14	20	100	48
50	16	1	100	46
-50	16	70	39	-43
50	16	20	82	43
25	16	15	97	43
25	18	1	100	39
50	18	1	100	39
-50	12	90	61	-39
50	12	50	90	33
-25	16	45	50	-31
-25	14	45	69	-31
-50	18	70	30	-31
50	18	20	61	31
25	18	15	71	31
-50	14	90	44	-30
-50	10	120	71	-29
-50	12	70	72	-28
50	12	20	100	28
25	14	15	100	26
50	14	1	100	26
25	12	45	97	25
-25	12	65	76	-24
50	14	50	64	23
-25	18	45	38	-22
-50	12	120	50	-22
-50	16	90	33	-21
-50	10	150	61	-20
50	10	100	81	20
-25	14	65	54	-19
50	10	50	100	19
25	10	75	99	18
25	16	1	100	18
50	16	1	100	18
-50	8	200	72	-17
50	8	150	89	17
25	14	45	69	17
50	16	50	47	16
-25	10	95	84	-16
-50	18	90	26	-15
-50	14	120	37	-15
-25	16	65	40	-14
-50	12	150	43	-13
50	12	100	57	13
-25	12	95	59	-13
-50	10	90	87	-13
-50	6	300	79	-12
50	6	250	91	12
25	12	75	69	12
-25	10	125	69	-12
50	18	50	36	12
25	16	45	50	12
-50	10	200	50	-11
50	10	150	61	11
-50	8	150	89	-11
25	8	125	100	11
50	8	100	100	11
-50	8	250	61	-11
50	8	200	72	11
-50	16	120	28	-11
-25	18	65	31	-10
-25	8	175	79	-10
-50	14	150	32	-9
50	14	100	42	9
-50	4	450	87	-9
50	4	400	97	9
-50	6	250	91	-9
50	6	200	100	9
-50	6	350	69	-9
50	6	300	79	9
-25	14	95	43	-9
25	18	45	38	8
25	10	125	69	8
25	14	75	50	8
25	6	225	99	8
-25	12	125	49	-8
-50	18	120	22	-8
-50	8	300	53	-8
50	8	250	61	8
-50	12	200	36	-8
50	12	150	43	8
25	8	175	79	8
-50	4	500	80	-8
50	4	450	87	8
-50	10	250	42	-7
50	10	200	50	7
-50	6	400	62	-7
50	6	350	69	7
-50	16	150	25	-7
50	16	100	31	7
-25	6	275	84	-7
-25	16	95	32	-6
-25	10	175	55	-6
-50	4	550	73	-6
50	4	500	80	6
-25	8	225	66	-6
25	16	75	37	6
-50	8	350	47	-6
50	8	300	53	6
25	6	275	84	6
-50	6	450	57	-6
50	6	400	62	6
25	12	125	49	6

Lithofacies L7

Free Water Level Elevation Change (ft)	*In situ* Porosity (%)	Height Above Free Water (ft)	Predicted Water Saturation (%)	Difference in Sw from Baseline Sw (Sw%)
50	18	1	100	58
-50	12	70	48	-52
50	12	20	100	52
50	16	1	100	51
-50	14	70	41	-46
50	14	20	87	46
-50	10	70	56	-44
50	10	20	100	44
25	14	15	100	43
50	14	1	100	43
-50	16	70	35	-39
50	16	20	75	39
25	16	15	89	39
-25	12	45	62	-38
25	18	1	100	36
50	18	1	100	36
-50	8	70	65	-35
50	8	20	100	35
-50	6	90	65	-35
-50	8	90	56	-35
-50	18	70	30	-34
50	18	20	64	34
25	18	15	76	34
-25	14	45	54	-33
25	12	15	100	33
50	12	1	100	33
50	6	50	92	31
-50	10	90	48	-30
50	4	50	100	29
-25	16	45	46	-29
-25	10	45	73	-27
50	8	50	79	27
-50	12	90	41	-26
25	16	1	100	25
50	16	1	100	25
-25	18	45	40	-25
-50	6	70	75	-25
50	6	20	100	25
-50	4	90	75	-25
-50	4	120	64	-24
50	10	50	68	23
-25	8	65	68	-23
25	6	45	98	23
25	10	15	100	22
50	10	1	100	22
-50	14	90	35	-22
-25	6	65	79	-21
-50	6	120	55	-21
50	12	50	58	20
-25	10	65	58	-20
25	8	45	84	20
-50	16	90	30	-19
-50	8	120	47	-18
50	14	50	50	17
-25	12	65	50	-17
25	10	45	73	17
-50	18	90	26	-16
-25	8	45	84	-16
-50	10	120	40	-15
-50	4	150	56	-15
50	4	100	71	15
50	16	50	43	15
-25	4	95	73	-15
-25	14	65	43	-14
25	12	45	62	14
25	4	75	84	13
-50	12	120	35	-13
-50	6	150	48	-13
50	6	100	61	13
25	14	1	100	13
50	14	1	100	13
50	18	50	37	13
-25	6	95	63	-13
-25	16	65	37	-12
25	14	45	54	12
-50	4	70	88	-12
25	4	45	100	12
50	4	20	100	12
25	6	75	72	11
-50	14	120	30	-11
-50	8	150	41	-11
50	8	100	52	11
-25	8	95	54	-11
-25	18	65	32	-11
25	16	45	46	11
25	8	75	62	10
-50	16	120	26	-10
-50	10	150	35	-10
50	10	100	45	10
25	8	15	100	9
50	8	1	100	9
-25	10	95	46	-9
25	18	45	40	9
-25	4	125	62	-9
-50	4	200	47	-9
50	4	150	56	9
25	10	75	53	8
-50	18	120	22	-8
-50	12	150	30	-8
50	12	100	39	8
-25	4	65	92	-8
-25	12	95	40	-8
-25	6	125	53	-8
-50	6	200	40	-8
50	6	150	48	8
25	12	75	46	7
-50	14	150	26	-7
50	14	100	33	7
-25	14	95	34	-7
-25	8	125	46	-7
-50	8	200	35	-6
50	8	150	41	6
25	4	125	62	6
25	14	75	39	6
-50	16	150	22	-6
50	16	100	29	6
-25	16	95	29	-6

Lithofacies L8

Free Water Level Elevation Change (ft)	*In situ* Porosity (%)	Height Above Free Water (ft)	Predicted Water Saturation (%)	Difference in Sw from Baseline Sw (Sw%)
50	18	1	100	42
50	18	1	100	25
50	18	20	75	28
50	18	50	53	12
50	18	100	41	6
50	16	1	100	42
50	16	1	100	23
50	16	20	77	31
50	16	50	53	13
50	16	100	40	6
50	14	1	100	41
50	14	1	100	20
50	14	20	80	34
50	14	50	53	14
50	14	100	39	6
50	12	1	100	40
50	12	1	100	16
50	12	20	84	39
50	12	50	54	15
50	12	100	38	7
50	10	1	100	39
50	10	1	100	11
50	10	20	89	44
50	10	50	54	17
50	10	100	37	7
50	8	1	100	38
50	8	20	96	52
50	8	50	54	19
50	8	100	35	8
50	6	1	100	36
50	6	20	100	58
50	6	50	54	22
50	6	100	33	8
50	4	1	100	34
50	4	20	100	59
50	4	50	55	25
50	4	100	30	9
25	18	1	100	25
25	18	15	83	25
25	18	45	55	8
25	16	1	100	23
25	16	15	87	28
25	16	45	56	9
25	14	1	100	20
25	14	15	91	32
25	14	45	56	10
25	12	1	100	16
25	12	15	97	37
25	12	45	56	11
25	12	75	44	6
25	10	1	100	11
25	10	15	100	39
25	10	45	57	12
25	10	75	43	6
25	8	15	100	38
25	8	45	58	14
25	8	75	42	7
25	6	15	100	36
25	6	45	58	16
25	6	75	40	8
25	4	15	100	34
25	4	45	60	19
25	4	75	38	8
-25	18	45	55	-19
-25	18	65	48	-10
-25	16	45	56	-22
-25	16	65	48	-10
-25	14	45	56	-24
-25	14	65	48	-11
-25	14	95	40	-6
-25	12	45	56	-28
-25	12	65	47	-13
-25	12	95	39	-6
-25	10	45	57	-32
-25	10	65	46	-14
-25	10	95	38	-7
-25	8	45	58	-38
-25	8	65	46	-16
-25	8	95	36	-8
-25	6	45	58	-42
-25	6	65	45	-19
-25	6	95	34	-8
-25	4	45	60	-40
-25	4	65	43	-23
-25	4	95	31	-9
-50	18	70	47	-28
-50	18	90	43	-15
-50	18	120	38	-9
-50	18	150	35	-6
-50	16	70	47	-31
-50	16	90	42	-16
-50	16	120	37	-9
-50	16	150	34	-6
-50	14	70	46	-34
-50	14	90	41	-18
-50	14	120	36	-10
-50	14	150	33	-6
-50	12	70	45	-39
-50	12	90	40	-20
-50	12	120	35	-11
-50	12	150	31	-7
-50	10	70	45	-44
-50	10	90	39	-22
-50	10	120	33	-11
-50	10	150	29	-7
-50	8	70	44	-52
-50	8	90	37	-25
-50	8	120	31	-13
-50	8	150	27	-8
-50	6	70	42	-58
-50	6	90	35	-28
-50	6	120	29	-14
-50	6	150	24	-8
-50	4	70	41	-59
-50	4	90	33	-33
-50	4	120	25	-15
-50	4	150	21	-9

Table 7.3.7.Summary of depth intervals and porosities by lithofacies for limestone that exhibit a water saturation change greater that 5% due to FWL elevation change. Intervals and porosities not shown exhibit < 5% Sw change due to elevation changes from -50 to +50 ft.

Lithofacies L6

Free Water Level Elevation Change (ft)	*In situ* Porosity (%)	Height Above Free Water (ft)	Predicted Water Saturation (%)	Difference in Sw from Baseline Sw (Sw%)
50	18	20	100	31
50	18	50	92	42
50	18	100	50	15
50	18	150	35	8
50	16	20	100	15
50	16	50	100	37
50	16	100	63	19
50	16	150	44	10
50	16	200	34	6
50	14	50	100	22
50	14	100	78	23
50	14	150	55	12
50	14	200	43	7
50	12	100	97	28
50	12	150	68	15
50	12	200	53	9
50	12	250	44	6
50	10	100	100	15
50	10	150	85	18
50	10	200	66	11
50	10	250	55	8
50	10	300	47	6
50	8	150	100	18
50	8	200	82	14
50	8	250	68	10
50	8	300	58	7
50	6	200	100	16
50	6	250	84	12
50	6	300	72	9
50	6	350	63	7
50	4	250	100	11
50	4	300	89	11
50	4	350	78	8
50	4	400	70	7
25	18	45	100	31
25	18	75	65	14
25	18	125	41	6
25	16	45	100	15
25	16	75	80	18
25	16	125	52	8
25	14	75	100	22
25	14	125	64	9
25	12	125	80	12
25	12	175	60	6
25	10	125	99	14
25	10	175	74	8
25	8	175	92	10
25	8	225	74	6
25	6	225	91	8
25	4	275	95	7
-25	18	65	73	-27
-25	18	95	53	-16
-25	18	125	41	-9
-25	16	65	91	-9
-25	16	95	66	-20
-25	16	125	52	-11
-25	16	175	39	-6
-25	14	95	81	-19
-25	14	125	64	-14
-25	14	175	48	-7
-25	12	125	80	-17
-25	12	175	60	-8
-25	10	175	74	-10
-25	10	225	60	-6
-25	8	175	92	-8
-25	8	225	74	-8
-25	6	225	91	-9
-25	6	275	77	-6
-25	4	325	83	-6
-50	18	70	69	-31
-50	18	90	55	-45
-50	18	120	43	-26
-50	18	150	35	-15
-50	18	200	27	-8
-50	16	70	85	-15
-50	16	90	69	-31
-50	16	120	54	-32
-50	16	150	44	-19
-50	16	200	34	-10
-50	16	250	28	-6
-50	14	90	85	-15
-50	14	120	67	-33
-50	14	150	55	-23
-50	14	200	43	-12
-50	14	250	35	-7
-50	12	120	83	-17
-50	12	150	68	-28
-50	12	200	53	-15
-50	12	250	44	-9
-50	12	300	38	-6
-50	10	150	85	-15
-50	10	200	66	-18
-50	10	250	55	-11
-50	10	300	47	-8
-50	10	350	41	-6
-50	8	200	82	-18
-50	8	250	68	-14
-50	8	300	58	-10
-50	8	350	51	-7
-50	6	250	84	-16
-50	6	300	72	-12
-50	6	350	63	-9
-50	6	400	57	-7
-50	4	300	89	-11
-50	4	350	78	-11
-50	4	400	70	-8
-50	4	450	63	-7

Lithofacies L9

Free Water Level Elevation Change (ft)	*In situ* Porosity (%)	Height Above Free Water (ft)	Predicted Water Saturation (%)	Difference in Sw from Baseline Sw (Sw%)
50	18	1	100	72
50	18	1	100	56
50	18	20	44	24
50	18	50	25	9
50	16	1	100	61
50	16	1	100	44
50	16	20	56	28
50	16	50	34	11
50	14	1	100	51
50	14	1	100	32
50	14	20	68	30
50	14	50	44	12
50	14	100	32	6
50	12	1	100	42
50	12	1	100	22
50	12	20	78	32
50	12	50	53	14
50	12	100	40	6
50	10	1	100	32
50	10	1	100	12
50	10	20	88	34
50	10	50	62	14
50	10	100	48	7
50	8	1	100	23
50	8	20	97	34
50	8	50	71	15
50	8	100	56	7
50	6	1	100	15
50	6	20	100	29
50	6	50	79	16
50	6	100	63	8
50	4	1	100	8
50	4	20	100	22
50	4	50	86	16
50	4	100	70	8
25	18	1	100	56
25	18	15	52	24
25	18	45	26	6
25	16	1	100	44
25	16	15	65	27
25	16	45	36	8
25	14	1	100	32
25	14	15	78	29
25	14	45	46	9
25	12	1	100	22
25	12	15	89	30
25	12	45	56	9
25	10	1	100	12
25	10	15	99	31
25	10	45	65	10
25	10	75	53	6
25	8	15	100	23
25	8	45	73	10
25	8	75	61	6
25	6	15	100	15
25	6	45	82	11
25	6	75	69	6
25	4	15	100	8
25	4	45	89	11
25	4	75	77	6
-25	18	45	26	-17
-25	18	65	21	-7
-25	16	45	36	-20
-25	16	65	30	-9
-25	14	45	46	-22
-25	14	65	39	-10
-25	12	45	56	-23
-25	12	65	48	-11
-25	12	95	41	-6
-25	10	45	65	-24
-25	10	65	56	-11
-25	10	95	49	-6
-25	8	45	73	-24
-25	8	65	65	-12
-25	8	95	57	-6
-25	6	45	82	-18
-25	6	65	73	-12
-25	6	95	64	-7
-25	4	45	89	-11
-25	4	65	80	-12
-25	4	95	71	-7
-50	18	70	20	-24
-50	18	90	17	-11
-50	18	120	14	-6
-50	16	70	28	-28
-50	16	90	25	-14
-50	16	120	21	-7
-50	14	70	37	-30
-50	14	90	33	-16
-50	14	120	29	-8
-50	14	150	26	-6
-50	12	70	46	-32
-50	12	90	41	-17
-50	12	120	37	-9
-50	12	150	33	-6
-50	10	70	55	-34
-50	10	90	50	-18
-50	10	120	45	-10
-50	10	150	41	-7
-50	8	70	63	-34
-50	8	90	58	-19
-50	8	120	52	-11
-50	8	150	48	-7
-50	6	70	71	-29
-50	6	90	65	-19
-50	6	120	60	-11
-50	6	150	56	-8
-50	4	70	78	-22
-50	4	90	73	-20
-50	4	120	67	-12
-50	4	150	62	-8

Table 7.3.8.Summary of depth intervals and porosities by lithofacies for fine- to medium-crystalline sucrosic dolomites that exhibit water saturation change greater that 5% due to FWL elevation change. Intervals and porosities not shown exhibit < 5% Sw change due to elevation changes from -50 to +50 ft.

		Hoobler		Graskell		Flower*	
	P	465	465	423	423	465	465
	Z	0.92	0.92	0.92	0.92	0.92	0.92
	Cgrv Perfs Reference	NA	NA	FWL+75	FWL+100	FWL+75	FWL+125
	Sim Model FWL	+65	-35	+30	+5	+145	+95
	Geomod 4-3 FWL	+20	+20	+44	+44	+142	+142

Shading indicates model used in simulation excercises.

OGIP (BCF) by Zone (Formation/Member level)

		Hoobler		Graskell		Flower*	
CHASE	**HRNGTN**	4	5	4	4	10	10
	KRIDER	29	31	13	13	47	46
	ODELL	0	0	4	4	1	1
	WINF	22	24	9	10	24	24
	GAGE	2	3	9	10	8	9
	TWND	40	48	31	32	32	31
	B/TWND	3	5	3	3	2	2
	FTRLY	24	42	64	65	32	31
	MATFIELD	0	0	2	3	2	2
	WREFORD	0	11	18	19	11	11
COUNCIL GROVE	**A1_SH**	0	0	1	2	0	0
	A1_LM	0	4	11	14	5	5
	B1_SH	0	0	0	0	0	1
	B1_LM	0	0	1	1	4	5
	B2_SH	0	0	0	0	0	0
	B2_LM	0	0	0	1	5	6
	B3_SH	0	0	0	0	0	0
	B3_LM	0	0	0	0	1	1
	B4_SH	0	0	0	1	0	0
	B4_LM	0	0	0	0	1	2
	B5_SH	0	0	0	0	0	0
	B5_LM	0	0	0	0	4	8
	C_SH	0	0	0	0	0	0
	C_LM	0	0	0	0	0	2
	Chase	124	169	155	161	169	167
	Council Grove	0	4	14	20	20	30
	Combined	124	173	169	181	189	197
	% change Chase		36.3%		3.8%		-1.2%
	% change Council Grove		#DIV/0!**		44.4%		50.0%
	% change combined		39.5%		7.1%		4.2%

* The two Flower models have more than one variable changing
** Hoobler has no gas in Council Grove or Wreford with higher FWL.

Table 7.3.9. Comparison of OGIP by zone in three multi-section simulation models as a function of the height above FWL. Relatively small changes in FWL dramatically affect zones lower in the section and very little in the very upper part of the Chase.

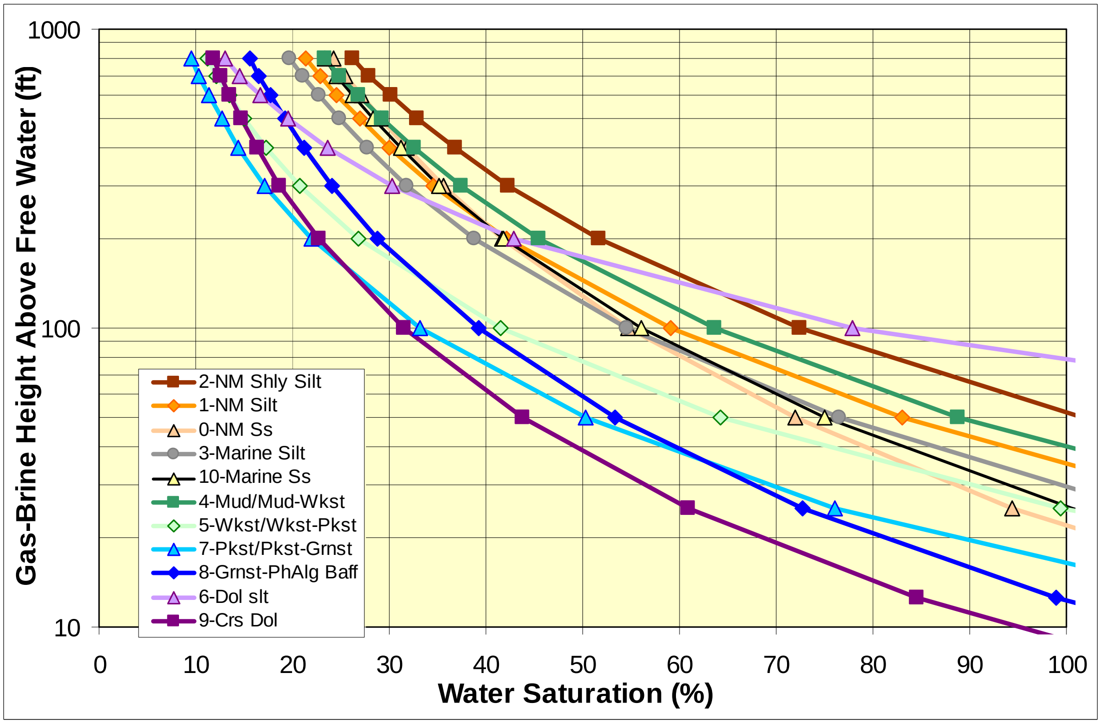

Figure 7.1.1. Model height above free water level curves for all 11 lithofacies for a ϕi = 10% rock. Water saturation can vary by up to 60% for the same porosity rock depending on the lithofacies. Curves were constructed using equations 4.2.15-4.2.19 in text. Differences in water saturation are greatest at lower heights and decrease with increasing height above free water level.

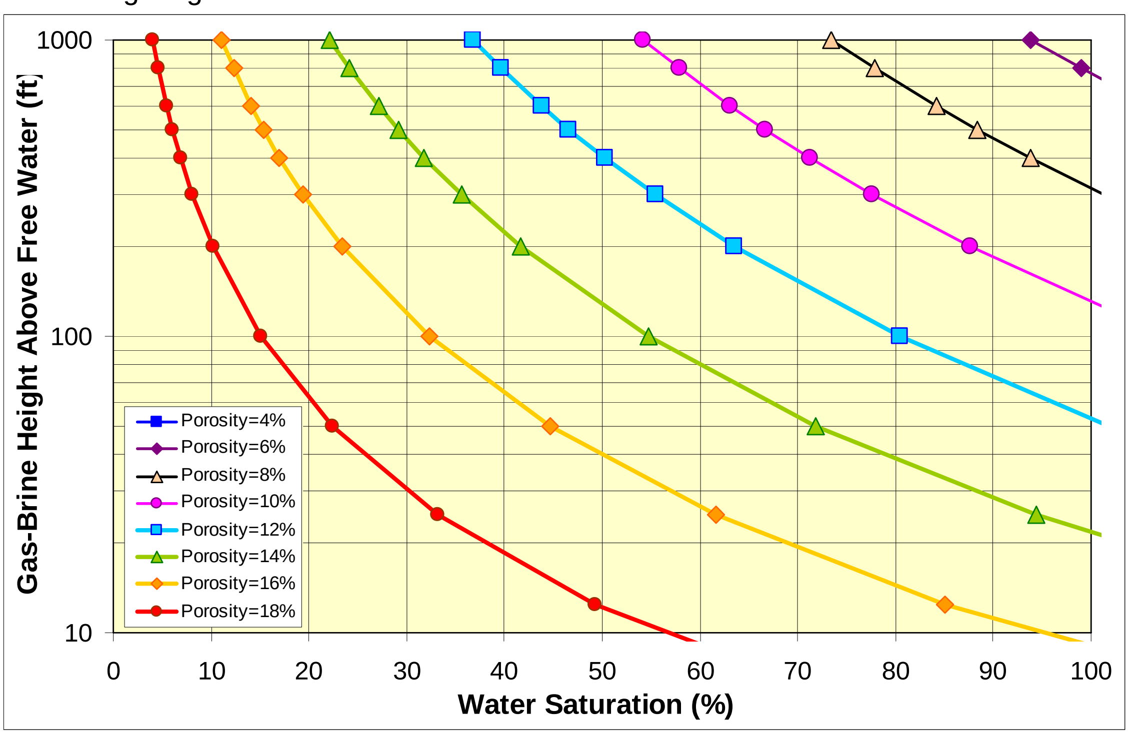

Figure 7.1.2. Model height above free water level curves for continental very fine to fine-grained sandstones (L0) constructed using equations 4.2.15-4.2.19 in text.

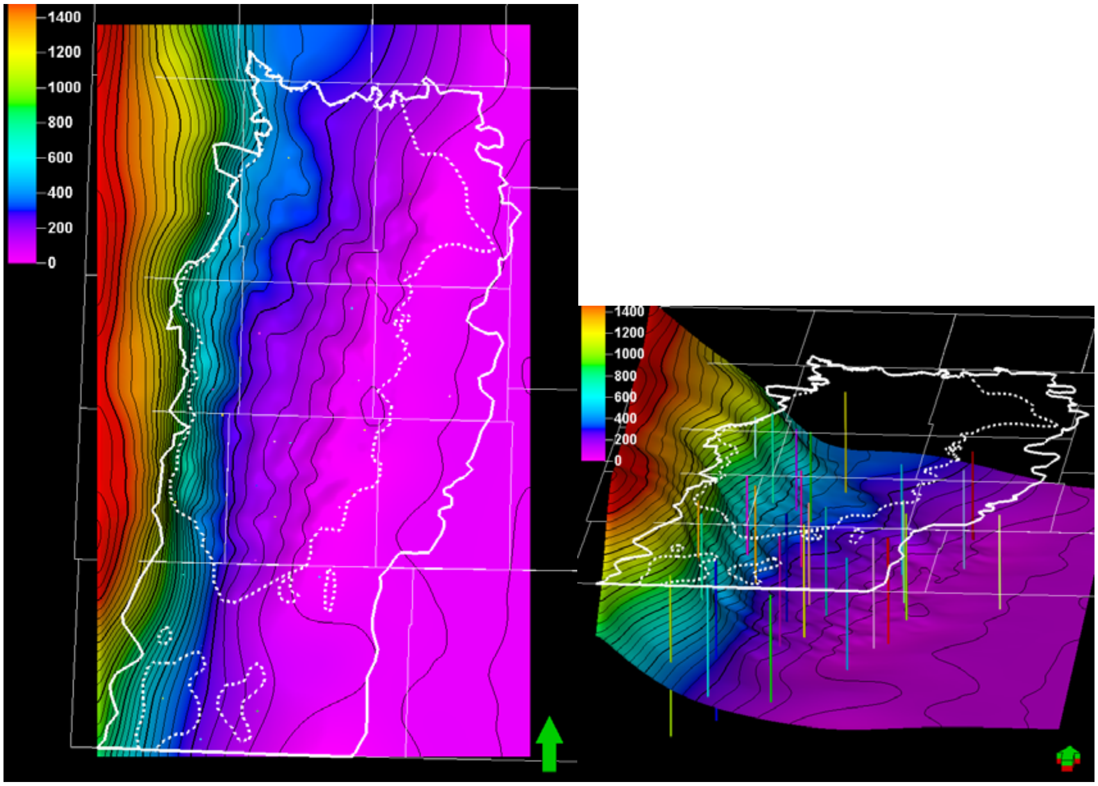

Figure 7.2.1. Two views of the FWL surface model version Geomod4 with a contour interval = 50 ft. The FWL surface is relatively flat on the east side (+50 at the Hugoton boundary to +20 at the Panoma boundary). The surface rises gradually to the midfield position and then rises rapidly to approximately +1000 at the west margin of the Hugoton.

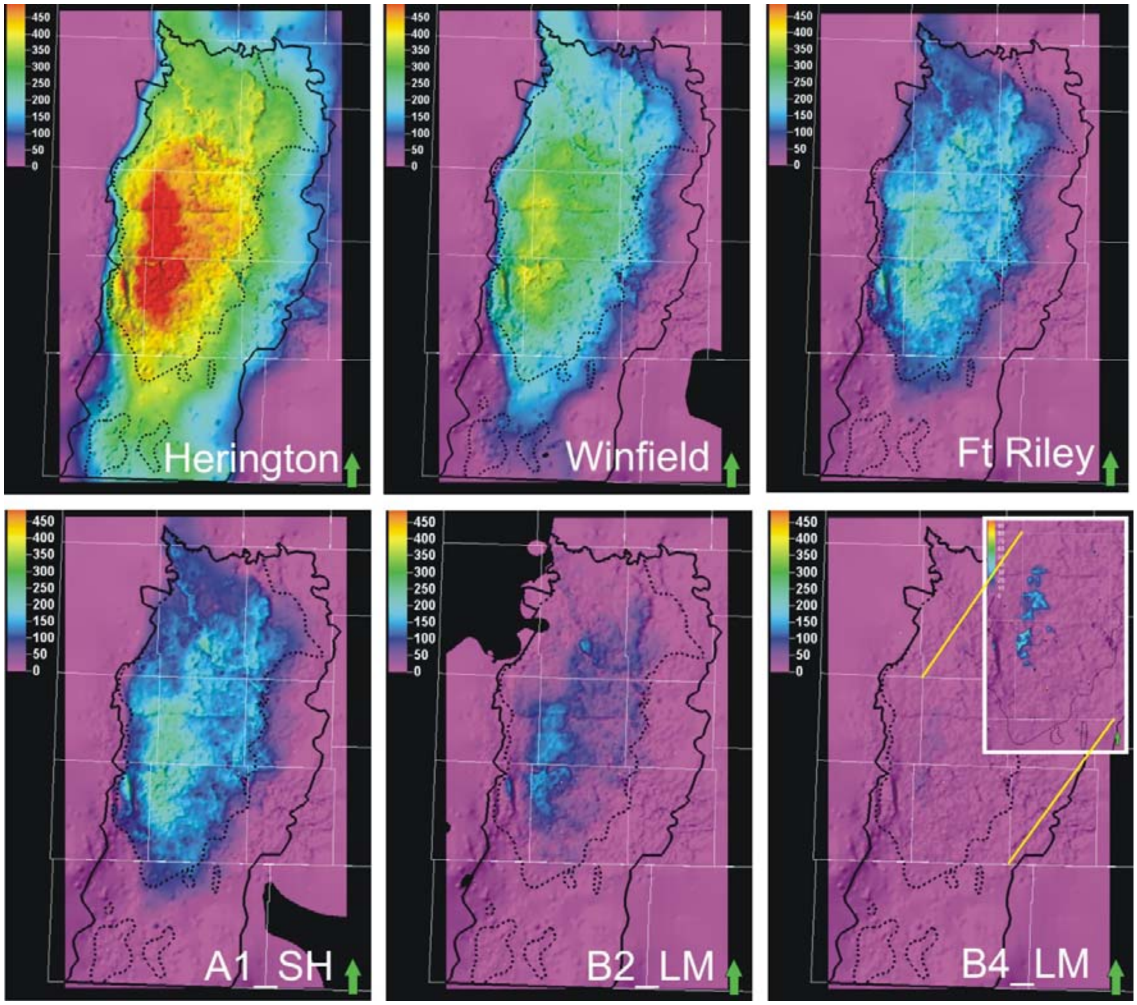

Figure 7.2.2. Height above FWL for key stratigraphic horizons in the Chase and Council Grove. Scale is from 0 to 500 ft (150 m) except for the B4_LM where the insert map covering Grant and Stevens Counties is 0-100 ft.

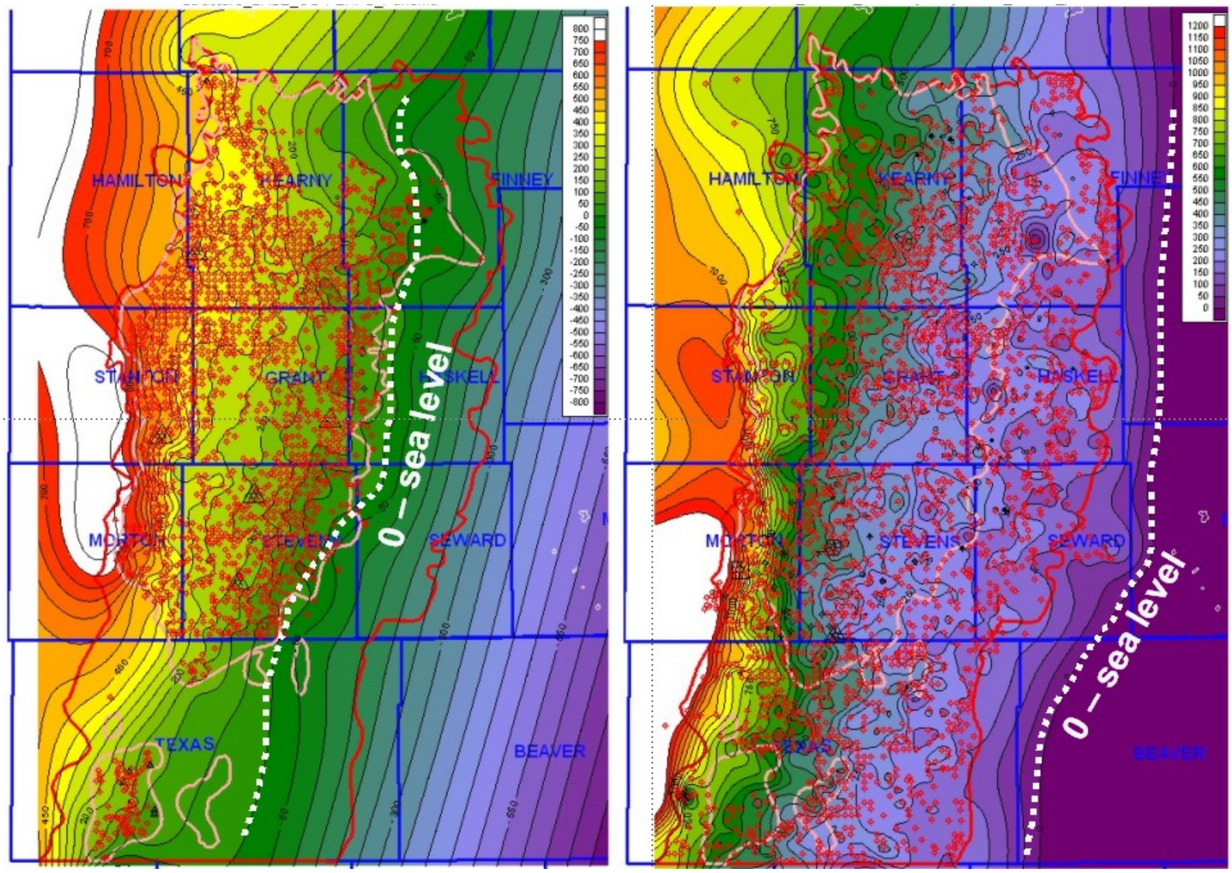

Figure 7.2.3. Elevation above sea level for base of Council Grove (Panoma) perforations, 2000 wells (left), and base of Chase (Hugoton) perforations, 4000 wells (right). Contour interval = 50 ft. Lowest perforations in the Council Grove at the Panoma margin approximately at sea level. In the Chase the perforations at the Hugoton margin are approximately 150-200 ft above sea level.

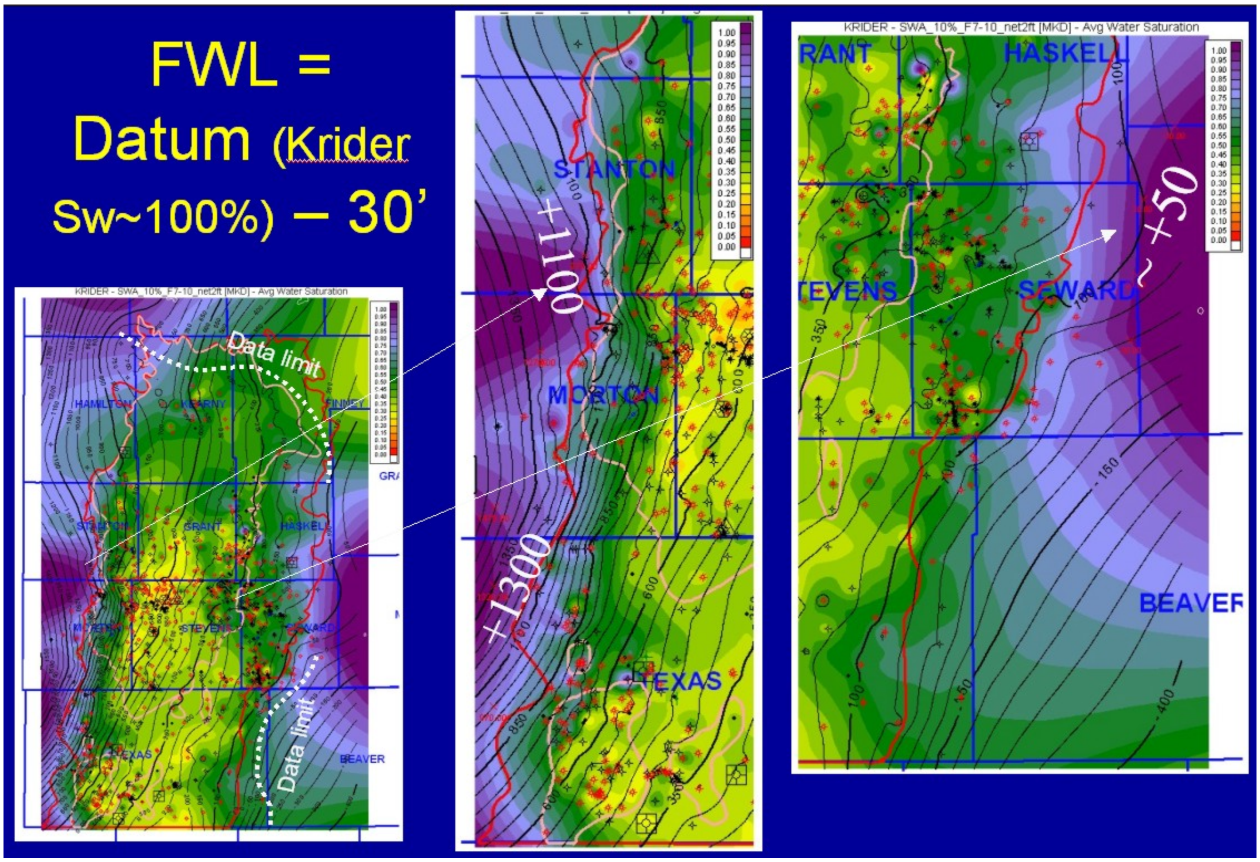

Figure 7.2.4 Average water saturation for Krider calculated from wireline logs using Archie for grain-supported lithofacies having porosity greater than 8% in color (purple is 100% Sw). Contour lines (50-ft interval) are the structure on the base of the Krider. Estimated FWL is 30 ft below coincidence of the base of Krider and 100% Sw.

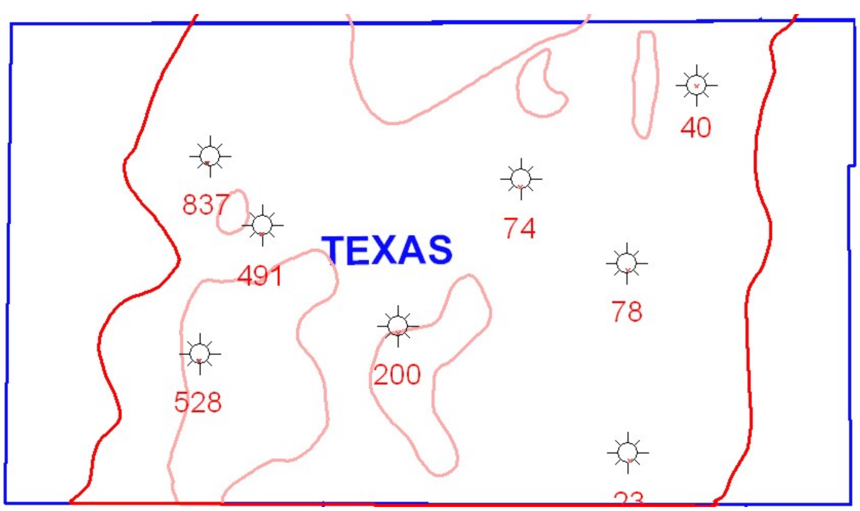

Figure 7.2.5. Back-calculated FWL for eight wells in Texas County, Oklahoma, in feet above sea level.

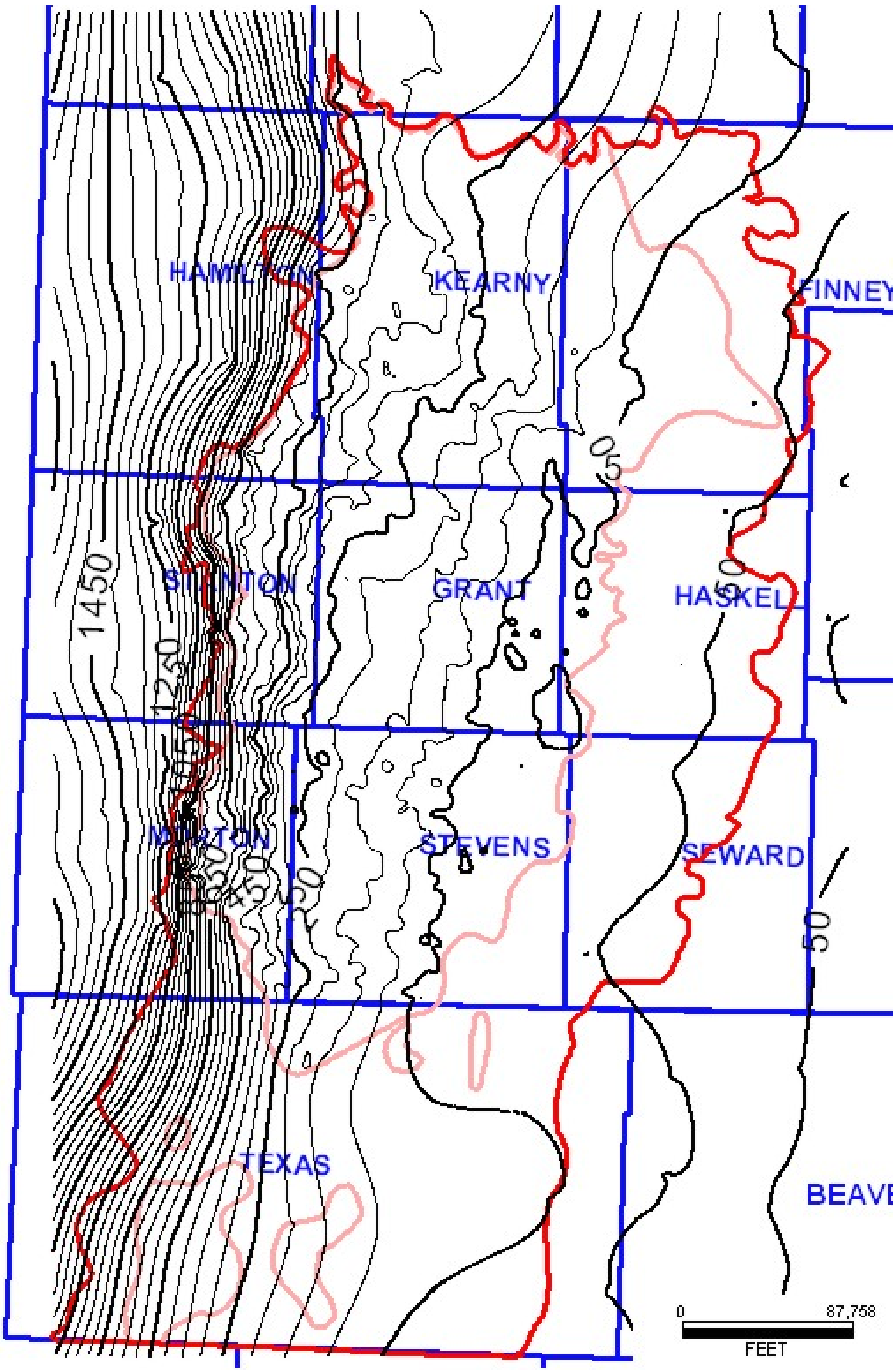

Figure 7.2.6 Geomod 4-3 FWL resulting from the integration of three methods.

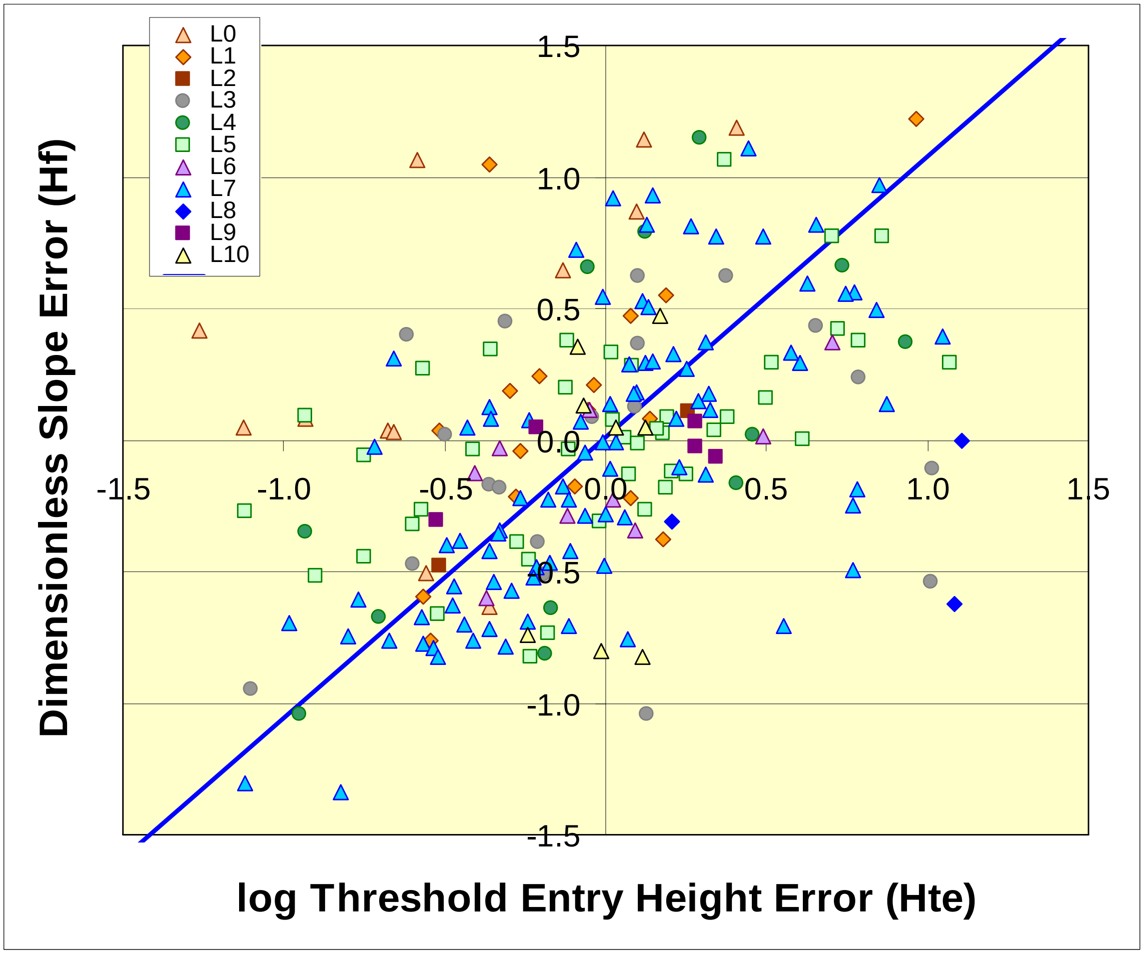

Figure 7.3.1. Crossplot of H_{afwl}-S_w curve parameter errors, logH_{te} error (threshold entry height parameter) versus, H_f error (dimensionless slope) for all lithofacies. Positive correlation between the two errors exhibits a reduced major axis line with slope=1.07 and intercept = 0.013.

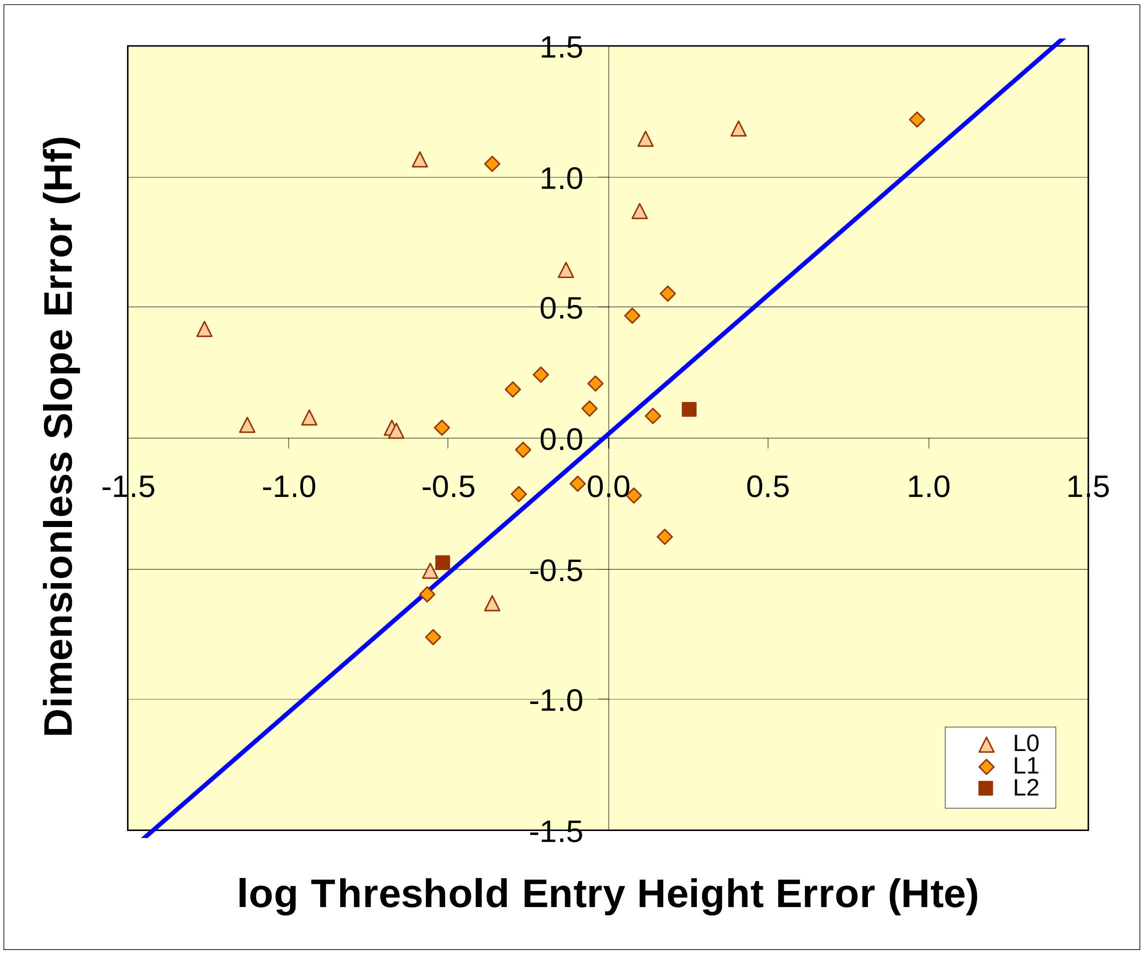

Figure 7.3.2. Crossplot of H_{afwl}-S_w curve parameter errors, logH_{te} error (threshold entry height parameter) versus, H_f error (dimensionless slope) for continental siltstone and sandstone lithofacies. Positive correlation between the two errors exhibits a reduced major axis line with slope=1.07 and intercept = 0.013.

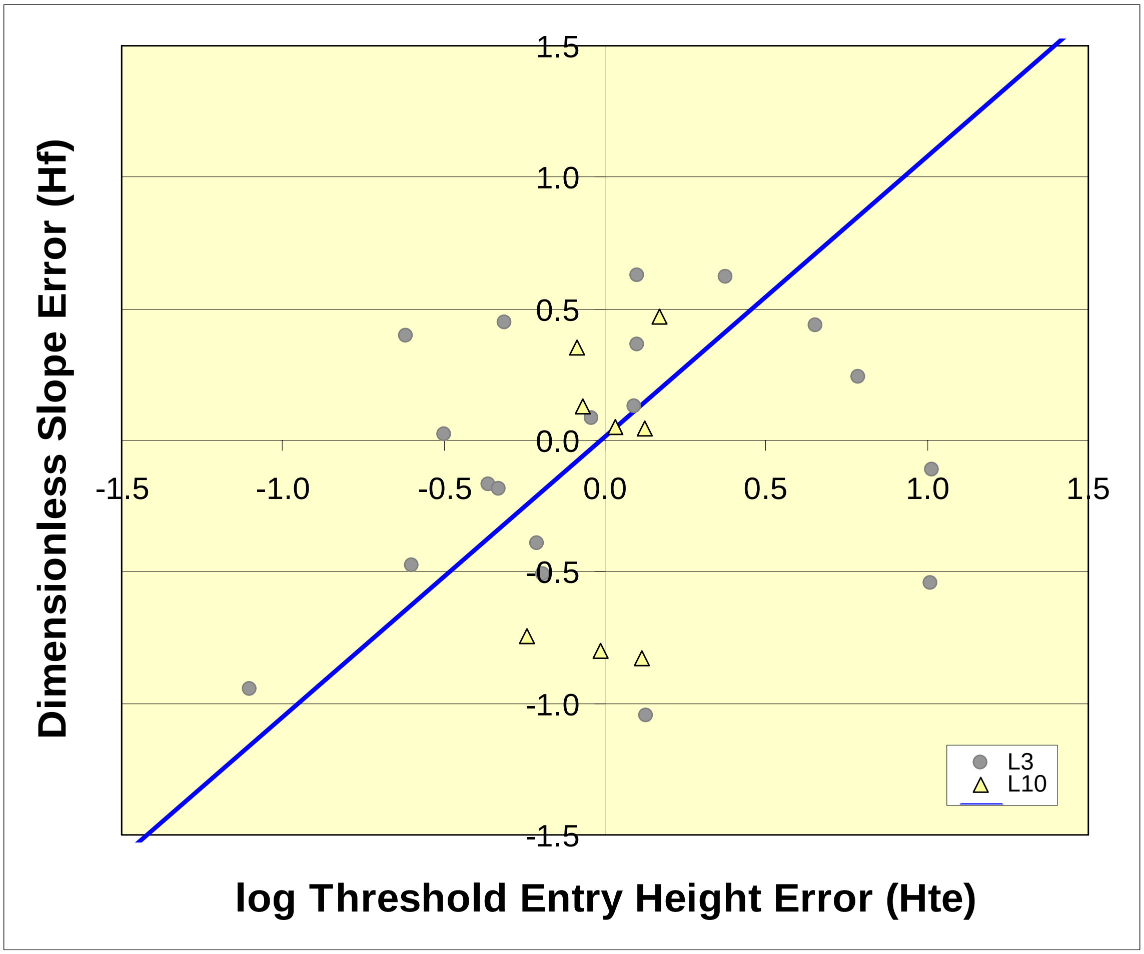

Figure 7.3.3. Crossplot of H_{afwl}-S_w curve parameter errors, logH_{te} error (threshold entry height parameter) versus, H_f error (dimensionless slope) for marine siltstone and sandstone lithofacies. Positive correlation between the two errors exhibits a reduced major axis line with slope=1.07 and intercept = 0.013.

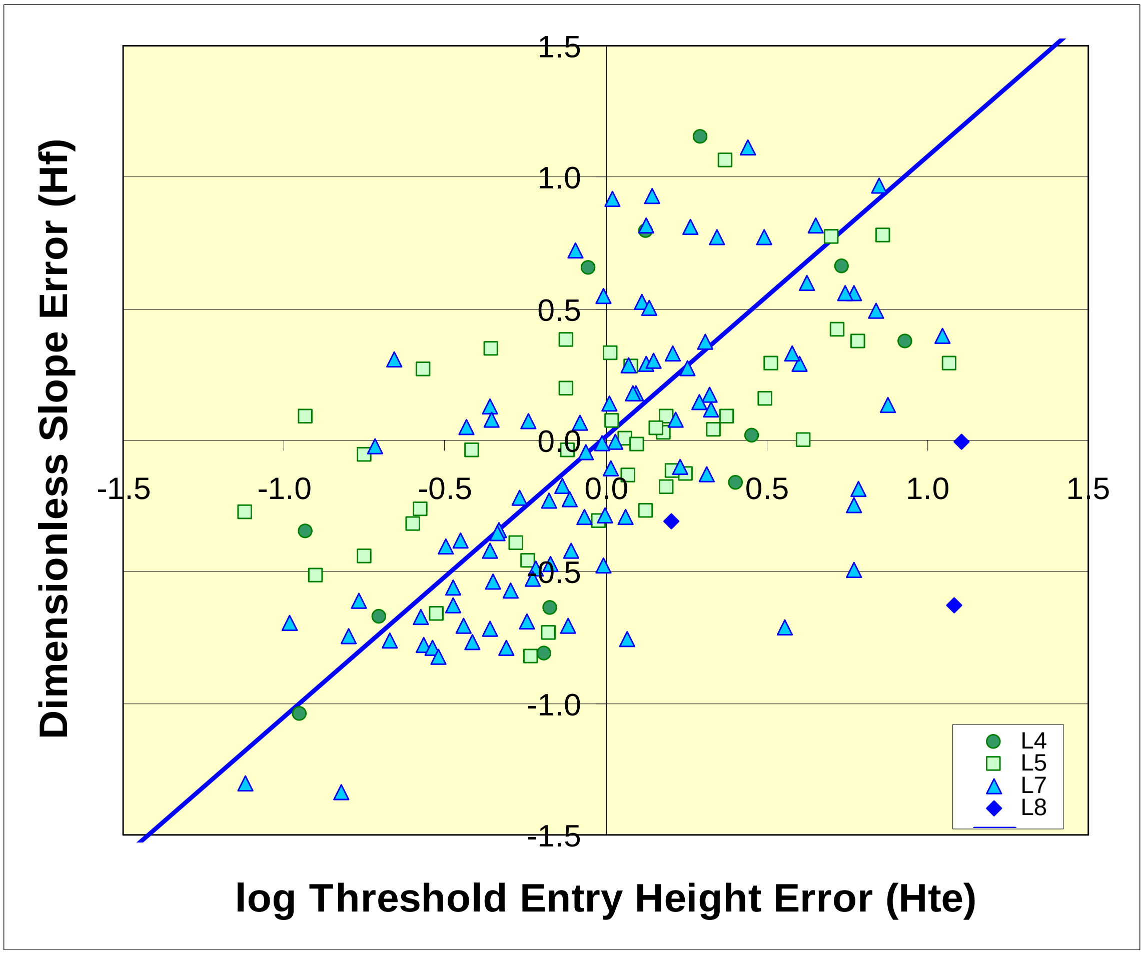

Figure 7.3.4. Crossplot of H_{afwl}-S_w curve parameter errors, logH_{te} error (threshold entry height parameter) versus, H_f error (dimensionless slope) for limestone lithofacies. Positive correlation between the two errors exhibits a reduced major axis line with slope=1.07 and intercept = 0.013.

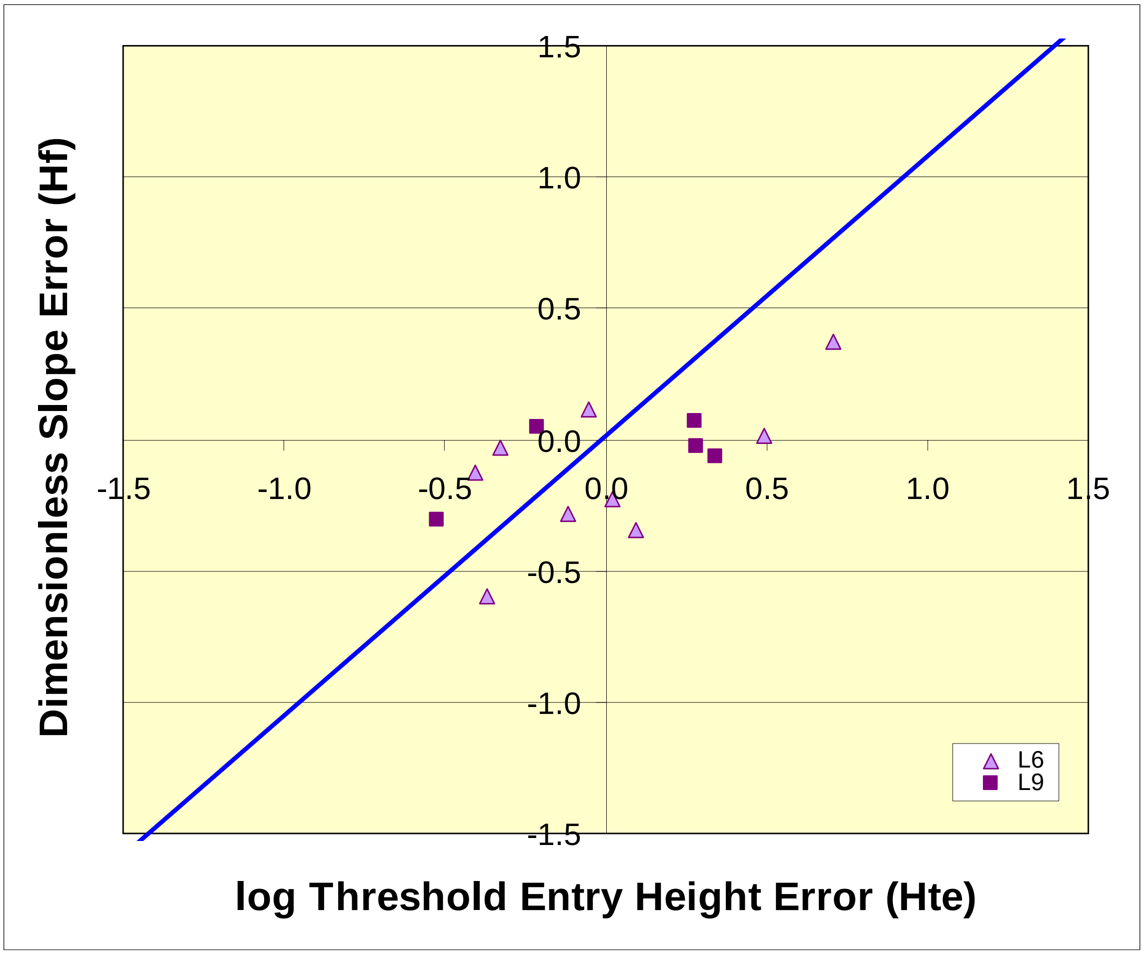

Figure 7.3.5. Crossplot of H_{afwl}-S_w curve parameter errors, logH_{te} error (threshold entry height parameter) versus, H_f error (dimensionless slope) for fine- to medium-crystalline sucrosic dolomite lithofacies. Positive correlation between the two errors exhibits a reduced major axis line with slope=1.07 and intercept = 0.013.

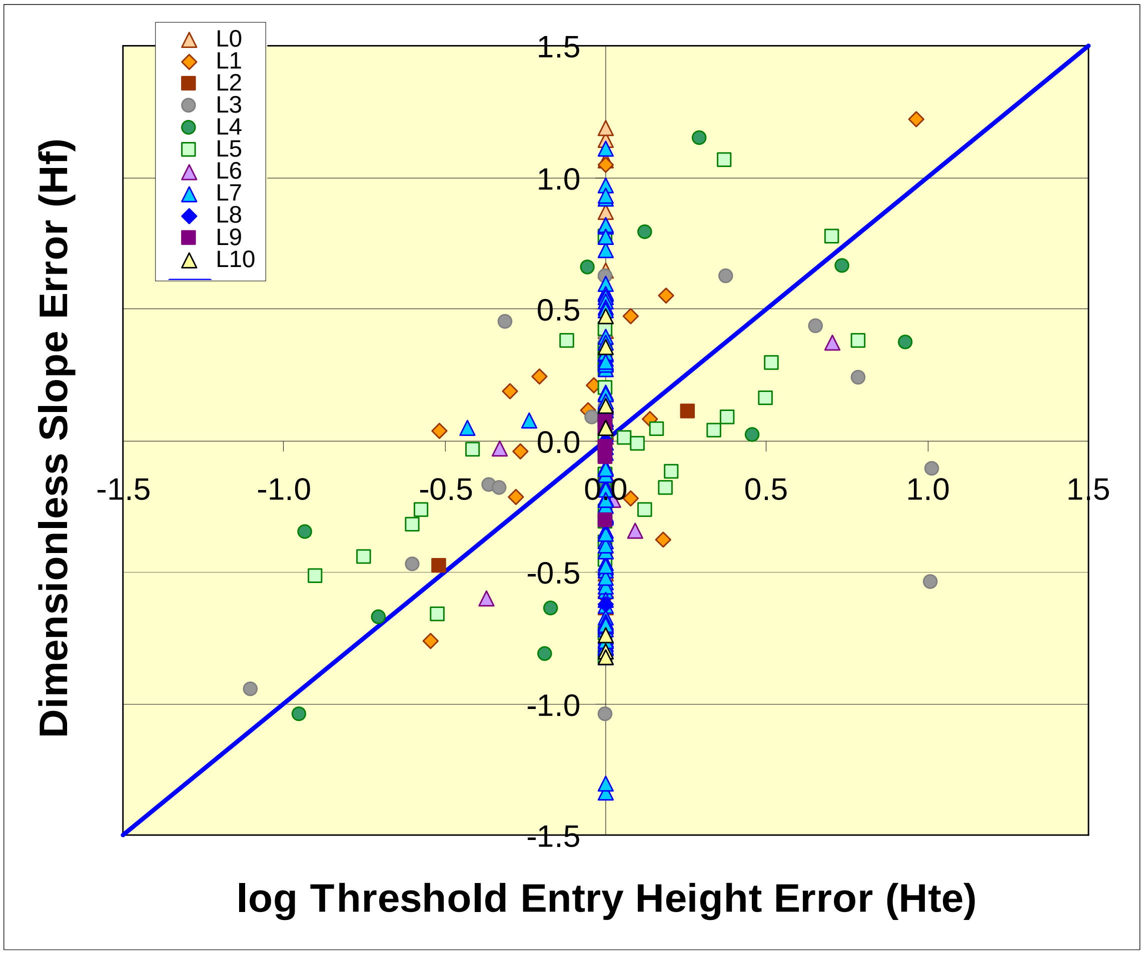

Figure 7.3.6. Crossplot of H_{afwl}-S_w curve parameter errors, logH_{te} error (threshold entry height parameter) versus, H_f error (dimensionless slope) for all lithofacies. Positive correlation between the two errors exhibits a reduced major axis line with slope=1.07 and intercept = 0.013. In the figure all samples in which the measured and predicted threshold entry height H_{te} is less than 50 ft were assigned an error of zero Because error in this range of threshold entry height is not significant.

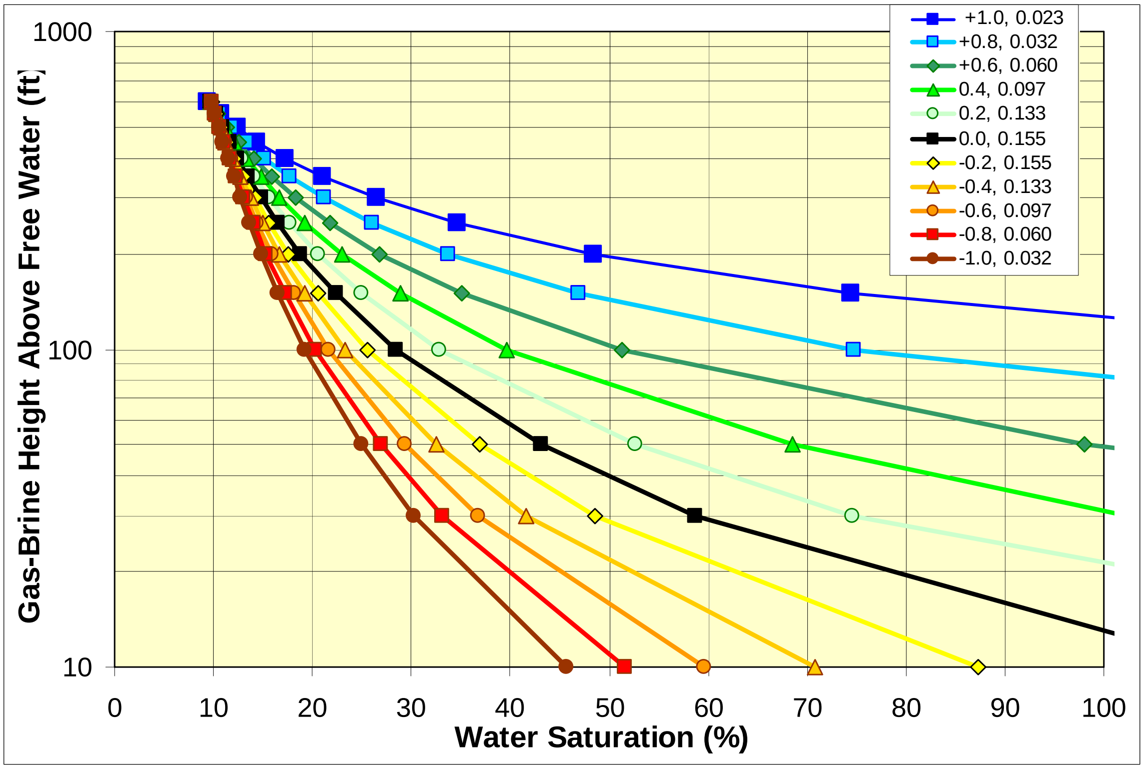

Figure 7.3.7. Example H_{afwl}-S_w curves for a packstone/grainstone with 16% porosity showing the range in curves produced by error in the parameters for creating the H_{afwl}-S_w curve. Highest and lowest curves represent -2 and +2 standard deviations on the parameter errors. Approximate fraction of total population for each curve is shown. Fractions were used to weight predicted saturations to sum a probability-weighted predicted saturation that is compared against the baseline model in the tables 7.3.1-7.3.4.

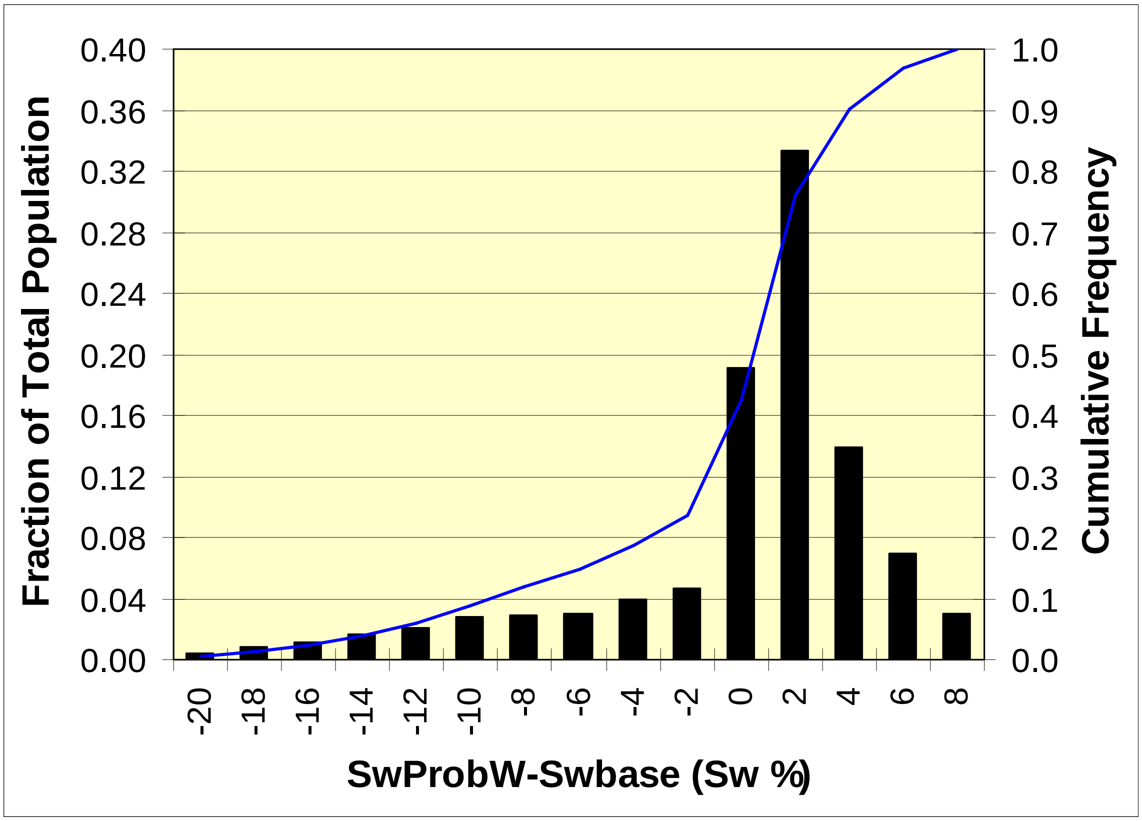

Figure 7.3.8. Frequency distribution of difference in saturation between probability-weighted saturations and baseline model saturations for selected porosity and height above free water level values shown in Tables 7.3.1-7.3.4 (n= 1,232).